Aalto University publication series
DOCTORAL DISSERTATIONS 164/2020

Coherent Thermal Machines: Fluctuations and Performance

Paul Menczel

A doctoral dissertation completed for the degree of Doctor of Science (Technology) to be defended, with the permission of the Aalto University School of Science, via remote connection on 11 November 2020 at 13:00.
Remote connection link: https://aalto.zoom.us/j/68824530640.

Aalto University
School of Science
Department of Applied Physics
Quantum Transport Group

Supervising professor
Professor Christian Flindt, Aalto University, Finland

Preliminary examiners
Dr. Gabriele De Chiara, Queen's University Belfast, United Kingdom
Dr. Martí Perarnau-Llobet, Max-Planck-Institute of Quantum Optics, Germany

Opponent
Professor Eric Lutz, University of Stuttgart, Germany

Aalto University publication series
DOCTORAL DISSERTATIONS 164/2020

ISBN 978-952-64-0087-7 (printed)
ISBN 978-952-64-0088-4 (pdf)
ISSN 1799-4934 (printed)
ISSN 1799-4942 (pdf)
http://urn.fi/URN:ISBN:978-952-64-0088-4

Unigrafia Oy
Helsinki 2020

Finland

Printed matter
4041-0619

Aalto University

Abstract

Aalto University, P.O. Box 11000, FI-00076 Aalto www.aalto.fi

Author
Paul Menczel

Name of the doctoral dissertation
Coherent Thermal Machines: Fluctuations and Performance

Publisher School of Science

Unit Department of Applied Physics

Series Aalto University publication series DOCTORAL DISSERTATIONS 164/2020

Field of research Quantum Thermodynamics

Manuscript submitted 11 June 2020 **Date of the defence** 11 November 2020

Permission for public defence granted (date) 20 August 2020 **Language** English

☐ **Monograph** ☒ **Article dissertation** ☐ **Essay dissertation**

Abstract

Quantum Engineering is a rapidly evolving discipline, promising the development of groundbreaking new technologies. To overcome the challenges posed by the nanoscopic scales and ultra-cold temperatures that are required for the implementation of quantum devices, understanding the thermodynamic interaction of these devices with their environment is important. Improving our knowledge of the laws of quantum thermodynamics enables engineers to exert better control over quantum circuits and it paves the way for more effective thermal management solutions on the nanoscale.

In this dissertation, we focus on the study of thermal machines such as heat engines or refrigerators. These devices have recently been miniaturized in labs to the point where quantum effects can influence their performance. Due to the well-known advantages of quantum over conventional computers, it is natural to wonder whether coherence effects might be able to give a similar performance enhancement to thermal machines. Here, we approach this question on three different levels. First, we study the theory of periodically controlled open quantum systems in order to better understand the mathematical foundations of reciprocating thermal devices. Second, we investigate transport phenomena in open quantum systems, enabling us to discuss the fluctuations of thermodynamic currents and how they affect the performance of thermal machines. Third, and finally, we examine whether the performance of quantum heat engines is subject to universal bounds and how these bounds change in different operation regimes.

The results of this thesis shed light on the optimal design of quantum devices, which will soon be ready for experimental implementation and investigation. Overall, we find that coherence leads to quantum friction, that is, to an increase in thermodynamic irreversibility with associated performance losses. In the adiabatic weak-coupling regime, these losses outweigh the benefits stemming from the increased number of degrees of freedom that are accessible in quantum setups. In other words, we find that coherence should generally be kept as small as possible in order to optimize the performance of nanoscale thermal machines in this regime. A promising direction for future investigations is to explore the effects of strong coupling and fast driving, where quantum advantages may be achievable.

Keywords Statistical Physics, Quantum Physics, Fluctuations and Noise, Thermal Machines, Open Quantum Systems, Counting Statistics, Optimization Problems

ISBN (printed) 978-952-64-0087-7 **ISBN (pdf)** 978-952-64-0088-4

ISSN (printed) 1799-4934 **ISSN (pdf)** 1799-4942

Location of publisher Helsinki **Location of printing** Helsinki **Year** 2020

Pages 154 **urn** http://urn.fi/URN:ISBN:978-952-64-0088-4

Preface

> The highest forms of understanding we can achieve are laughter and human compassion
>
> *Richard Feynman*

The work presented in this thesis was performed in the Quantum Transport group at the Department of Applied Physics of Aalto University. I am happy that I had the opportunity to spend the four years of my doctoral studies in Finland, a beautiful country and a great environment for living and doing research. Of course, these four years have had their ups and downs, and I think that 2020 in particular has been a challenging year for everyone. But, apparently, I have managed to finish this thesis, and now I am excited to move on to my first postdoctoral position!

First of all, I wish to thank Kay Brandner for contacting me at just the right time after my Master's degree, where I had done a little detour into High Energy Physics, encouraging me to "return to my roots" and come work on Quantum Thermodynamics in Helsinki. Thank you, Kay, also for the incredible amount of support with both Physics itself and academia in general. Of course, I am also very grateful towards my supervisor, Christian Flindt, for welcoming me into the Quantum Transport group and for providing me with valuable opportunities to connect with other research groups through conferences and joint projects. Big thanks for their great teamwork go to Fredrik Brange, Shilpi Singh and Dmitry Golubev, who were my closest collaborators on some of the papers included in this thesis, and to Tuomas Pyhäranta and Eetu Loisa, the students that I have had the honor of supervising.

I thank my pre-examiners, Martí Perarnau-Llobet and Gabriele De Chiara, for taking the time to carefully read this dissertation and providing valuable feedback. Let me also thank in advance Eric Lutz, who has agreed to be the opponent in my virtual defense. I wish it were possible to meet in person at Aalto University!

For never allowing a day at the office to be boring, thank you to all of the QTies: Aydin, Fredrik, Kay, Pablo, Pedro, Tony, and especially Elina, who helped me settle in and feel at home (using large amounts of Fafa's). Thanks also to Jukka Pekola and his PICO group, who always have an open ear for theorists such as myself. I am grateful to Franco Nori, who kindly hosted me in his group at RIKEN, Japan, for four months in 2019, and to Keiji Saito, whom I was able

to visit during this time. I also thank Keiko, who was a huge support to me in this foreign country, as well as all the other great people I have met during my stay at RIKEN, including my collaborators Neill Lambert and Ken Funo.

A very special thanks decorated with unicorns goes to Erika! So happy to be friends whatever continents we may be on, and we owe each other visits as soon as possible!

Last but not least, I am deeply grateful to my parents who have supported me throughout my studies, even if I may struggle to make my research understandable for non-Physicists sometimes. I shall try harder!

Helsinki, October 7, 2020,

Paul Menczel

Contents

List of Publications

This thesis consists of an overview and of the following publications which are referred to in the text by their Roman numerals.

I P. Menczel and K. Brandner. Limit cycles in periodically driven open quantum systems. *J. Phys. A: Math. Theor.* **52** 43LT01, September 2019.

II F. Brange, P. Menczel, and C. Flindt. Photon counting statistics of a microwave cavity. *Phys. Rev. B* **99**, 085418, February 2019.

III S. Singh, P. Menczel, D. S. Golubev, I. M. Khaymovich, J. T. Peltonen, C. Flindt, K. Saito, É. Roldán, and J. P. Pekola. Universal First-Passage-Time Distribution of Non-Gaussian Currents. *Phys. Rev. Lett.* **122**, 230602, June 2019.

IV P. Menczel, C. Flindt, and K. Brandner. Quantum jump approach to microscopic heat engines. *Phys. Rev. Research* **2**, 033449, September 2020.

V P. Menczel, C. Flindt, and K. Brandner. Thermodynamics of cyclic quantum amplifiers. *Phys. Rev. A* **101**, 052106, May 2020.

VI P. Menczel, T. Pyhäranta, C. Flindt, and K. Brandner. Two-stroke optimization scheme for mesoscopic refrigerators. *Phys. Rev. B* **99**, 224306, June 2019.

Author's Contribution

Publication I: "Limit cycles in periodically driven open quantum systems"

The author performed all derivations, created all figures and drafted the manuscript.

Publication II: "Photon counting statistics of a microwave cavity"

The author performed the derivations presented in Apps. A, B and F and contributed to the derivations presented in Apps. C - E. The author drafted Apps. A, B and F and contributed to the preparation of the remaining manuscript.

Publication III: "Universal First-Passage-Time Distribution of Non-Gaussian Currents"

The author performed the numerical calculations leading to the solid curves in Figs. 3 and 4 and in the figures in the supplemental material. The author wrote Sec. 1 of the supplement and contributed to the derivation of the approximate model described on page 3.

Publication IV: "Quantum jump approach to microscopic heat engines"

The author contributed to the derivations and to the preparation of the manuscript, and wrote App. B.

Publication V: "Thermodynamics of cyclic quantum amplifiers"

The author performed all derivations and calculations. The author created Figs. 2 and 3 and contributed to the creation of Fig. 1. The author drafted the manuscript excluding Secs. I and V and the abstract.

Publication VI: "Two-stroke optimization scheme for mesoscopic refrigerators"

The author was the main supervisor of the student, T. Pyhäranta, who derived the results presented in Sec. 3 and in the appendix as his Bachelor's thesis. The author performed all other derivations and calculations. The author drafted the manuscript excluding Secs. IV and VI.

List of Figures

Symbols

$\hbar$	Reduced Planck's constant
k_B	Boltzmann's constant
$\mathbb{1}$	Identity operator
$\sigma_{x,y,z}$	Pauli matrices
a, $a^\dagger$	Ladder operators of the harmonic oscillator
ρ, p	System state operator, populations
H	System Hamiltonian
V	Unitary transformation
$\hbar\omega$, ε	Level splittings
$\hbar\Delta$	Qubit tunneling energy
U	Internal energy
W, Q	Work output, heat input
η	Efficiency, coefficient of performance
S	Entropy
T, β	Temperature, inverse temperature $\beta = 1/(k_B T)$
$\bar{n}$, $\bar{n}_\mathrm{F}$	Bose-Einstein factor, Fermi-Dirac factor
$\bar{T}$	Cycle time
$\hat{L}$, $\hat{D}$	Lindblad generator, Lindblad dissipator
γ^μ, V^μ	Coupling rate, Lindblad jump operator
τ_E, τ_S, $\bar{\tau}$, τ_D	Time scales, cf. Sec. 2.2
$\mathbb{T}$	Jump trajectory
X, x	Counting variable, increment
χ	Counting field
$\mathscr{M}$, $\mathscr{K}$	Moment-generating function, cumulant-generating function
j	Average jump rate

Time dependence is denoted by subscripts and time derivatives by dots. Hats indicate superoperators. The natural logarithm is written as log.

1. Introduction

The discovery of the laws of quantum physics in the early 20th century was one of the greatest scientific achievements of our time. Without it, modern life and technology as we know it would be inconceivable. The development of computers and smart devices relies on the knowledge of the electronic band structures in semiconductors. An increasing understanding of nanoscale biological processes as well as the application of new imaging and radiologic techniques has expanded the possibilities of medicine. And instant global communication has become possible due to lasers sending coherent light pulses through optical fibers around the world.

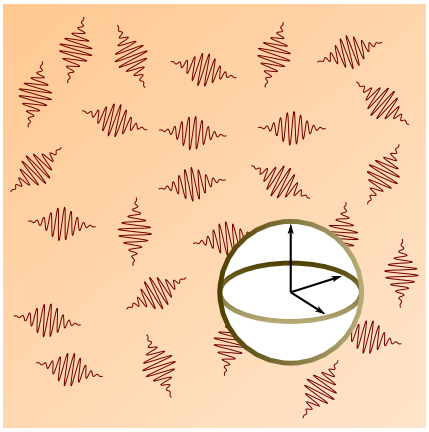

Figure 1.1. The term open quantum system denotes quantum systems that are not isolated [1]. Rather, they are influenced by their environment, which exhibits a meso- or macroscopic amount of degrees of freedom. Here, the open quantum system is schematically depicted as a Bloch sphere embedded in a thermal environment.

This development is continuing to have a great impact on technology today. A new discipline, quantum information technology, has emerged [2], promising the development of quantum-enhanced cryptographic tools and computers, which perform fundamentally *better* than their conventional counterparts [3]. The implementation of quantum devices however raises difficult technological challenges, ranging from the problem of decoherence [4] to the demand for effective thermal management on the nanoscale [5]. Decoherence stands for the universal tendency of quantum devices to quickly lose their coherence, that is, their "quantumness", when in contact with the macroscopic world. This phenomenon is the result of the incoherent, random interaction of a quantum system with its environment, which can never be completely avoided. It is therefore crucial to understand the behavior of open quantum systems quantitatively in theoretical models, see Fig. 1.1.

The theory of open quantum systems has been the subject of intensive research since the 1970s [6]. Initially, this research focused on describing their dynamics

in the Markovian regime, where system and environment are clearly separated entities and the back-action of the system on the environment is negligible. In the last decade, studies have started to explore new lines of research, including the investigation of the thermodynamics of the system-reservoir interaction in the Markovian regime [7–9] and beyond [9–11]. This research aims to understand how coherence affects the laws of thermodynamics on the smallest scales, and thus shed light on fundamental problems in quantum mechanics and quantum information theory.

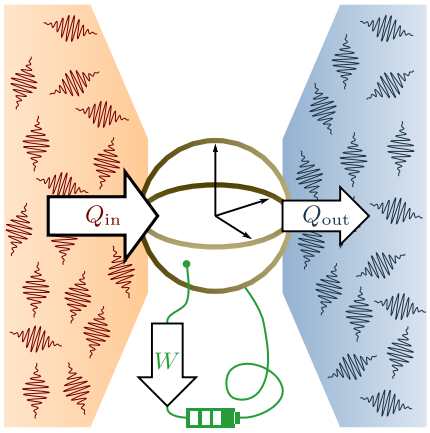

Figure 1.2. Basic setup of a quantum heat engine. The open quantum system, here depicted as a Bloch sphere, plays the role of the working substance of the engine. A hot thermal reservoir provides the heat Q_{in} and the waste heat Q_{out} is deposited into a cold reservoir. External driving manipulates the working substance, thereby extracting the work $W = Q_{\text{in}} - Q_{\text{out}}$.

Thermal machines, such as heat pumps, heat engines or refrigerators, are central objects of study in both classical and quantum thermodynamics [9, 12]. A heat engine, for example, takes advantage of a thermal gradient in its environment in order to convert thermal energy into useful work, see Fig. 1.2. While, traditionally, heat engines are machines as large as the steam engines of the industrial revolution, these devices have recently been miniaturized by many orders of magnitude and can now be implemented in the lab using superconducting qubits [13], single atoms [14] or single spins [15] as their working substance. The goal of this process is not only to improve our understanding of quantum thermodynamics, but also to guide the development of efficient cooling solutions for technological applications [5, 16].

Due to the advantages of quantum over classical computers, it is natural to wonder whether coherently working thermal machines might exhibit similar advantages over their macroscopic relatives. Initially, this discussion was sparked by the observation that the Carnot bound, which is a universal upper limit on the efficiency of heat engines in classical thermodynamics, could be overcome by exploiting coherence in the thermal reservoirs [17]. This analysis did however not take the cost of preparing the non-thermal reservoir state into account [18, 19]; in fact, quantum heat engines with thermal reservoirs can not work at efficiencies larger than the Carnot efficiency [20–22]. Breaking Carnot's law is not even possible for devices based on Maxwell's demons as long as the energy required to record the demon's information is factored in [23, 24].

Moving thus from the discussion of efficiency on to other thermodynamic performance indicators, coherence effects have been found sometimes advantageous [25–31] and sometimes detrimental [32–38] for the operation of thermal machines, depending on the specific application. These apparently contradictory results stem from the difficulty of clearly pointing out and quantifying quan-

tum effects in physical systems [39]. Typically, it is not possible to uniquely assign a classical counterpart to a quantum heat engine in order to compare their performance. The aim of this dissertation is therefore to investigate the impact of coherence on the performance of thermal machines in scenarios where performance gains and losses can be clearly distinguished. We approach this topic on three different levels, which correspond to the three main chapters of the overview.

In Chapter 2, we study the mathematical foundations of periodically operating open quantum systems. We first set up the adiabatic Lindblad framework for describing the dynamics of slowly driven, Markovian open quantum systems in the weak-coupling regime. The example of a damped qubit illustrates the available control operations and demonstrates the relaxation process in which the qubit decoheres and thermalizes with its environment. In Sec. 2.4, we proceed to discuss the relaxation process of periodically driven systems. We summarize Publication I, in which a sufficient condition for the complete relaxation of reciprocating devices is derived.

Chapter 3 is devoted to the general study of the statistics of quantum transport processes, such as the energy transport between system and reservoirs in thermal machines. The energy is transferred stochastically in discrete amounts, corresponding to quantum jumps of the system. Here, we introduce the formalism of quantum jump trajectories in order to derive the full counting statistics of quantum jumps and of transport quantities. Following Publication II and Publication III, we then apply the theory to concrete examples, which provide physical insight into transport phenomena and the impact of quantum effects.

In Chapter 4, we establish the framework of quantum thermodynamics in the weak-coupling regime and investigate the performance of quantum thermal machines. We discuss the results of the following three publications. First, in Publication IV, we extend bounds from the realm of classical non-equilibrium thermodynamics to the quantum regime in order to study how the strictness of the bounds increases with the system coherence. Second, in Publication V, we study a class of quantum heat engines without classical analoga and derive a surprisingly strong condition on the required complexity of the working substance. Third, in Publication VI, we examine a quantum microcooler, a concrete example of a quantum thermal machine, and compare the optimal operation protocols for this system as a function of the coherence.

Finally, we conclude and discuss future perspectives in Chapter 5.

2. Open Quantum Systems

2.1 Setup

In this chapter, we discuss the general theory of open quantum systems. Our total setup, the "universe", consists of a small quantum system and its large environment [1]. Later on, the small system will play the role of the working fluid of a thermal machine, and the environment that of one or several thermal reservoirs.

The quantum state of the universe is represented by a time-dependent state operator ρ_t^{tot} on the total Hilbert space

$$\mathscr{H}_{\text{tot}} = \mathscr{H} \otimes \mathscr{H}_{\text{env}}, \tag{2.1}$$

which consists of the system Hilbert space $\mathscr{H}$ and the environment Hilbert space $\mathscr{H}_{\text{env}}$. Due to the large number of degrees of freedom in the environment, its state is typically not experimentally accessible. Hence, we focus on the small system, whose state ρ_t can be obtained by applying a partial trace over the environment,

$$\rho_t = \text{tr}_{\text{env}}\, \rho_t^{\text{tot}}. \tag{2.2}$$

The effects of the environment will thus only be visible to the extent that they affect the time evolution of the system state.

The state of the universe evolves unitarily according to the von Neumann equation

$$\dot{\rho}_t^{\text{tot}} = \frac{1}{\mathrm{i}\hbar}[H_t^{\text{tot}}, \rho_t^{\text{tot}}], \tag{2.3}$$

where the total Hamiltonian H_t^{tot} has the form

$$H_t^{\text{tot}} = H_t \otimes \mathbb{1} + H_t^{\text{int}} + \mathbb{1} \otimes H^{\text{env}}. \tag{2.4}$$

Here, H_t, H_t^{int} and H^{env} are the system, the interaction and the environment Hamiltonian. We allow H_t to depend on time in order to model time-dependent external driving, for example in the form of external magnetic fields that are

applied to the setup. Also the interaction term H_t^{int} may depend on time, describing reservoirs that can be dynamically coupled and decoupled from the working system.

Given concrete expressions for the Hamiltonians, the equation of motion of the system state can be derived from the von Neumann equation. Assuming that system and reservoir are prepared in an uncorrelated state at the initial time $t_0 = 0$, this procedure generally leads to time evolution equations of the form [40, 41]

$$\dot{\rho}_t = \int_0^t \hat{K}_{t,\tau}\, \rho_\tau \, \mathrm{d}\tau. \tag{2.5}$$

Here, the memory kernel $\hat{K}_{t,\tau}$ is a superoperator acting on the system state. Note that we denote superoperators with hats throughout. Equation (2.5) shows that the evolution of the system state generally depends on its entire history; it is non-Markovian. In order to treat the non-Markovian dynamics exactly, it is typically assumed that the environment consists only of non-interacting Gaussian modes [42]. Then, a number of theoretical methods can be applied to the problem, including the framework of non-equilibrium Green's functions [43], the reaction coordinate framework [44, 45], and techniques based on the Feynman-Vernon influence functional representation [46–50].

These methods are valuable tools for the implementation of numerical simulations of non-Markovian open system dynamics. However, the system-environment interaction is very complex in general and strong correlations can make the distinction between system and environment fuzzy. To obtain a deeper, analytical understanding, we here follow a different approach and assume that the time evolution is Markovian. In practice, this assumption is often well justified; Markovian master equations play an important role for applications in most areas of modern quantum physics [51].

2.2 Markovian Open Quantum Systems

The dynamics of an open quantum system is called Markovian if it is memoryless, i.e., if the behavior of the system state does not depend on the history of its time evolution. This notion can be formalized in terms of the following three requirements [52]. First, the evolution from any initial time t_1 to a later time $t_2 \geq t_1$ can be described in terms of a propagator $\hat{U}_{t_2,t_1}$ such that $\rho_{t_2} = \hat{U}_{t_2,t_1}\, \rho_{t_1}$. The propagators are convex linear maps on the space of Hermitian, positive operators with unit trace. Second, the propagators satisfy $\hat{U}_{t,t} = \hat{\mathbb{1}}$, and the composition property

$$\hat{U}_{t_3,t_2}\, \hat{U}_{t_2,t_1} = \hat{U}_{t_3,t_1} \tag{2.6}$$

holds for all times $t_1 \leq t_2 \leq t_3$. Third, the propagators are required to be completely positive. In other words, $\hat{U}_{t_2,t_1} \otimes \hat{\mathbb{1}}_N$ must be a positive linear map, where the dimension N of the identity superoperator is arbitrary. These requirements

are satisfied if and only if the system state obeys the master equation [52–54]

$$\dot{\rho}_t = \hat{L}_t \rho_t \tag{2.7}$$

with a generator $\hat{L}_t$ of the form

$$\hat{L}_t \bullet = \frac{1}{\mathrm{i}\hbar}[H_t, \bullet] + \sum\nolimits_\mu \gamma_t^\mu \left(V_t^\mu \bullet V_t^{\mu\dagger} - \frac{1}{2}\left\{ V_t^{\mu\dagger} V_t^\mu, \bullet \right\} \right). \tag{2.8}$$

Here, H_t is a Hermitian operator, which is typically identified with the system Hamiltonian defined in Eq. (2.4). The sum enumerates dissipation channels with corresponding coupling rates $\gamma_t^\mu \geq 0$ and Lindblad operators V_t^μ, and $\{\bullet, \bullet\}$ is the anti-commutator.

Equation (2.7) is called the (time-inhomogeneous) Lindblad master equation [1, 51]. It is a generalization of the original Lindblad equation

$$\dot{\rho}_t = \hat{L} \rho_t, \tag{2.9}$$

which was derived by Gorini, Kossakowski, Sudarshan and Lindblad in 1976 [55, 56] for time-homogeneous Markovian systems with $\hat{U}_{t_2,t_1} = \hat{U}_{t_2-t_1}$. The generalized equation with time-dependent Lindblad generator allows for time-dependent reservoir couplings and external driving.

The derivation of Markovian master equations from the microscopic theory introduced in Sec. 2.1 generally requires a clear separation of time scales. The central assumption is that, after a perturbation, system-environment correlations decay and the state of the environment returns quickly to an equilibrium state. It is therefore unable to retain information on the history of the system evolution. Specifically, the time scale τ_E of the environmental reset is assumed to be short compared with $\bar{\tau}$, the time scale of the environment-induced dynamics of the system [52],

$$\tau_E \ll \bar{\tau}. \tag{2.10}$$

In terms of the microscopic model, the time scale $\bar{\tau}$ is given by $\bar{\tau} = \hbar E_{\mathrm{int}}^{-1}$, where E_{int} is the scale of the interaction term H^{int}. In other words, it is the time scale on which the system state changes in the interaction picture with respect to the system Hamiltonian.

For time-inhomogeneous setups, the Markov assumption (2.10) is generally not yet sufficient to guarantee the validity of a Lindblad equation; additional assumptions have to be made. In this thesis, we focus on the adiabatic weak-coupling framework [37, 57, 58], which relies on the assumptions of weak coupling, $E_{\mathrm{int}} \ll \hbar\tau_S^{-1}$, and slow driving, $\tau_D \gg \tau_E, \tau_S$. Here, τ_S is the time scale of the unperturbed system dynamics and τ_D the time scale of the external driving. That is, τ_D is the shortest time scale on which the total Hamiltonian and the equilibrium state of the environment vary. These assumptions can be summarized in the form of the time scale hierarchy

$$\tau_E, \tau_S \ll \bar{\tau}, \tau_D. \tag{2.11}$$

We note that other time scale hierarchies can also lead to Lindblad equations. For example, the limit $\tau_E \ll \bar{\tau}, \tau_S$ corresponds to quantum Brownian motion [1] and the regime of fast driving can be treated using the Floquet-Lindblad formalism [59]. Because the thermodynamic interpretation of these Lindblad equations varies from regime to regime, we choose to focus on the adiabatic weak-coupling regime only.

Since the environment in our setup corresponds to a thermal reservoir, the equilibrium state of the environment is the canonical state

$$\rho_t^{\mathrm{env,eq}} = \frac{1}{Z_t^{\mathrm{env}}} \exp[-\beta_t H^{\mathrm{env}}], \tag{2.12}$$

where $\beta_t = 1/(k_{\mathrm{B}} T_t)$ is the inverse temperature and $Z_t^{\mathrm{env}} = \mathrm{tr} \exp[-\beta_t H^{\mathrm{env}}]$ the partition function. Recall that the temperature T_t of the environment changes on the time scale $T_t/\dot{T}_t \sim \tau_D$, which is much longer than its reset time τ_E. In the adiabatic weak-coupling framework, the Lindblad generator then satisfies the following two conditions, which are together called the (quantum) detailed balance condition [6, 60]. First, the Lindblad operators are raising or lowering operators with respect to the instantaneous system Hamiltonian,

$$[H_t, V_t^\mu] = \varepsilon_t^\mu V_t^\mu, \tag{2.13}$$

where ε_t^μ is the change of the system energy induced by the jump operator V_t^μ. Second, the Lindblad operators come in pairs of raising and lowering operators. For every dissipation channel with Lindblad operator V_t^μ, there is thus another dissipation channel with the adjoint Lindblad operator $V_t^{\mu\dagger}$. The corresponding rate $\gamma_t^{\mu\dagger}$ satisfies

$$\gamma_t^{\mu\dagger} = \exp[\beta_t \varepsilon_t^\mu] \gamma_t^\mu, \tag{2.14}$$

i.e., the coupling rate of the excitation channel is suppressed with respect to the coupling rate of the emission channel by the Boltzmann factor.

For systems that are simultaneously coupled to multiple thermal reservoirs, the Lindblad generator has the form

$$\hat{L}_t \bullet = \frac{1}{\mathrm{i}\hbar}[H_t, \bullet] + \sum\nolimits_m \hat{D}_t^m \bullet, \tag{2.15}$$

where the index m runs over the reservoirs. Each dissipation superoperator $\hat{D}_t^m$ consists of a sum of dissipation channels like in Eq. (2.8), which satisfy detailed balance with respect to the inverse temperatures β_t^m of the respective reservoirs.

As an immediate consequence of the detailed balance condition, we find [60]

$$\hat{D}_t^m \rho_t^{\mathrm{eq}}[\beta_t^m] = 0, \tag{2.16}$$

where

$$\rho_t^{\mathrm{eq}}[\beta] = \frac{1}{Z_t[\beta]} \exp[-\beta H_t] \tag{2.17}$$

is the instantaneous canonical state of the system corresponding to the inverse temperature β and $Z_t[\beta] = \mathrm{tr} \exp[-\beta H_t]$ the partition function. In a time-homogeneous system coupled to a single reservoir, the thermal equilibrium state

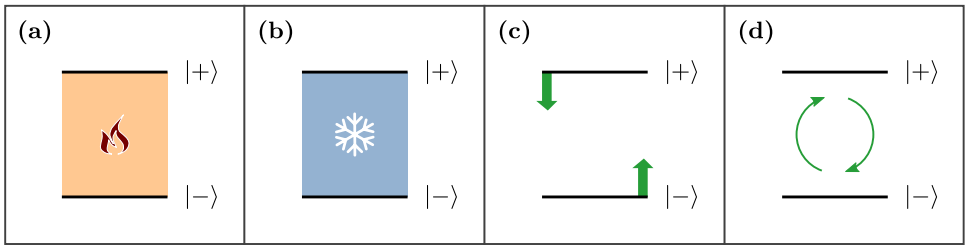

Figure 2.1. Each panel contains the schematic representation of an elementary control operation for a damped qubit. The thick horizontal lines symbolize the two energy eigenstates. (a), (b) The qubit thermalizes with a hot or cold thermal reservoir. (c) The level splitting of the qubit is reduced while the reservoir is decoupled. (d) The populations of the two states are swapped by applying a π pulse.

$\rho^{\mathrm{eq}}[\beta]$ is therefore a steady state. In a setup with multiple reservoirs, steady states generally do not have the form (2.17); instead, they are non-equilibrium steady states, which are harder to characterize.

2.3 Controlling a Qubit

We now illustrate the concepts introduced above on the basis of a simple example, the damped qubit. Qubits are quantum systems with two states $|+\rangle$ and $|-\rangle$ and can be realized experimentally for example using superconducting circuits [13, 61] or nuclear spins [62]. The Hamiltonian of a qubit can generally be written in the form

$$H_t = \frac{\hbar\omega_t}{2} V_t \sigma_z V_t^\dagger, \tag{2.18}$$

where $\hbar\omega_t$ is the level splitting, V_t the unitary transformation diagonalizing H_t, and $\sigma_z = |+\rangle\langle+| - |-\rangle\langle-|$ the Pauli matrix. When the qubit is in contact with a thermal reservoir at the inverse temperature β_t, its state evolves according to the Lindblad equation [1]

$$\begin{aligned}\dot\rho_t = \frac{1}{\mathrm{i}\hbar}[H_t,\rho_t] &+ \gamma_t(\bar n_t+1)\left(\sigma_t^\downarrow\rho_t\sigma_t^\uparrow - \frac{1}{2}\left\{\sigma_t^\uparrow\sigma_t^\downarrow,\rho_t\right\}\right)\\ &+ \gamma_t\bar n_t\left(\sigma_t^\uparrow\rho_t\sigma_t^\downarrow - \frac{1}{2}\left\{\sigma_t^\downarrow\sigma_t^\uparrow,\rho_t\right\}\right).\end{aligned} \tag{2.19}$$

Here, $\sigma_t^\uparrow = V_t|+\rangle\langle-|V_t^\dagger$ and $\sigma_t^\downarrow = V_t|-\rangle\langle+|V_t^\dagger$ are the instantaneous raising and lowering operators, γ_t is the characteristic rate of reservoir-induced excitations and emissions, and $\bar n_t = (\exp[\hbar\omega_t\beta_t]-1)^{-1}$ is the Bose-Einstein factor.

Even though this master equation describes only a single qubit, the resulting dynamics can be very complex. In order to gain intuition for its behavior, it is, however, often enough to understand a small number of elementary control operations, shown in Fig. 2.1. More complex protocols are obtained by combining multiple elementary operations. In the rest of this section, we discuss these elementary operations in detail.

Thermalization. In a thermalization stroke, depicted in Figs. 2.1(a) and 2.1(b), the system thermalizes with a reservoir at a constant temperature T. During

this operation, no other driving is applied to the system. The Hamiltonian H, the coupling rate γ and the Bose-Einstein factor $\bar{n}$ are therefore constant throughout the stroke.

To determine the time evolution of the state operator, we work in the eigenbasis of the Hamiltonian, i.e., $V = \mathbb{1}$. It is convenient to parametrize ρ_t in terms of the Bloch vector [1],

$$\rho_t = \frac{1}{2}\begin{pmatrix} 1+z_t & x_t - \mathrm{i}y_t \\ x_t + \mathrm{i}y_t & 1-z_t \end{pmatrix}. \tag{2.20}$$

Here, x_t, y_t and z_t are the components of the Bloch vector. Using the Lindblad equation (2.19), we derive the Bloch equations [1]

$$\begin{aligned} \dot{x}_t &= -\frac{\gamma}{2}(1+2\bar{n})\,x_t - \omega_t\, y_t, \\ \dot{y}_t &= -\frac{\gamma}{2}(1+2\bar{n})\,y_t + \omega_t\, x_t \quad \text{and} \\ \dot{z}_t &= -\gamma(1+2\bar{n})\,z_t - \gamma. \end{aligned} \tag{2.21}$$

The coherences x_t and y_t oscillate while decaying exponentially with the rate $\gamma(1+2\bar{n})/2$. The z-component of the Bloch vector, which describes the populations, approaches the equilibrium value $z^{\mathrm{eq}} = -(1+2\bar{n})^{-1}$ at long times. The state of the system at long times is thus independent of the initial conditions.

Classical Driving. In a classical driving stroke, depicted in Fig. 2.1(c), the level splitting $\hbar\omega_t$ of the qubit is changed. Throughout the stroke, the system is decoupled from the reservoir and the eigenvectors of the Hamiltonian remain constant.

The populations of the state operator stay constant during this operation, since

$$\langle n|\dot{\rho}_t|n\rangle = \frac{1}{\mathrm{i}\hbar}\langle n|[H_t,\rho_t]|n\rangle = 0, \tag{2.22}$$

where $|n\rangle$ denotes an eigenvector of the Hamiltonian. Further, since $[H_t,\dot{\rho}_t]=0$, a diagonal state operator remains diagonal. If a control protocol only consists of thermalization and classical driving strokes, the state at long times will therefore always be diagonal.

Coherent driving. In a coherent driving stroke, the system is decoupled from the reservoir and the level splitting remains constant [63]. This type of driving can create coherence in the system.

Consider for example the resonant Rabi Hamiltonian

$$H_t = \frac{\hbar\omega}{2}\,\mathrm{e}^{\mathrm{i}Xt}\,\sigma_z\,\mathrm{e}^{-\mathrm{i}Xt} \quad \text{with} \quad X = \frac{1}{2}\big(\Omega\,\sigma_x - \omega\,\sigma_z\big). \tag{2.23}$$

Here, Ω is the Rabi frequency and $\sigma_x = |+\rangle\langle -| + |-\rangle\langle +|$. Applied to the initial state $\rho_0 = |-\rangle\langle -|$, the time evolution generates coherent oscillations between the ground state and the excited state,

$$\langle +_t|\rho_t|+_t\rangle = \sin[\Omega t/2]^2 \quad \text{and} \quad \big|\langle +_t|\rho_t|-_t\rangle\big|^2 = \sin[\Omega t]^2/4, \tag{2.24}$$

where $|\pm_t\rangle = e^{iXt}|\pm\rangle$ are the time-dependent energy eigenstates.

Applying this control operation for the duration $\pi\Omega^{-1}$ swaps the populations of the two states. This operation thus corresponds to the application of a π pulse, depicted in Fig. 2.1(d).

2.4 Relaxation to Equilibrium

In our analysis of the thermalization of a damped qubit, we found that the system is relaxing, i.e., that its long-time behavior becomes independent of the initial conditions. Relaxation is a typical feature of Lindblad master equations. In this section, we discuss the mathematical properties of the generator $\hat{L}_t$ that lead to this behavior.

To this end, we first review the situation for open quantum systems described by time-homogeneous Lindblad equations. Here, the relaxation behavior of the system is mathematically characterized by an algebraic condition which was formulated by Spohn in 1977 [64]. Spohn's theorem states that the system is relaxing if the linear span $\mathcal{V}$ of the set of Lindblad operators is self-adjoint and irreducible. In this context, self-adjoint means that $V^\dagger$ is an element of $\mathcal{V}$ for each $V \in \mathcal{V}$, and irreducible means that any operator commuting with all of $\mathcal{V}$ must be a multiple of the identity. Intuitively, the condition of irreducibility requires the dissipative terms of the Lindblad equation to "connect" all states of the system, see Fig. 2.2. The self-adjointness condition excludes pathological situations arising at zero temperature.

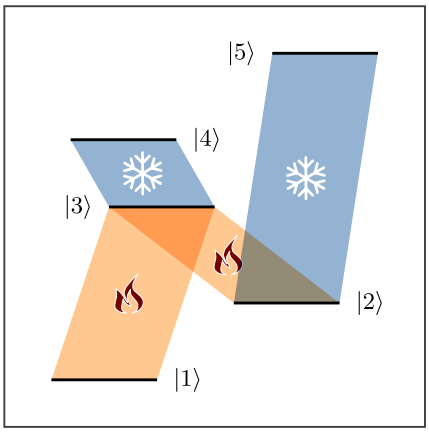

Figure 2.2. Illustration of Spohn's theorem. The diagram represents the thermalization process of a 5-level quantum system. Each shaded area in the diagram represents a pair of dissipation channels, which enable transitions between the two connected states. The system dynamics is thus given by a time-homogeneous Lindblad equation with eight Lindblad operators; they are $|1\rangle\langle 3|$, $|2\rangle\langle 3|$, $|2\rangle\langle 5|$, $|3\rangle\langle 4|$ and their adjoints. Since all states in the diagram are connected, the system is relaxing.

Spohn's theorem applies to any Lindblad equation of the form (2.9). We now present a short, instructive proof of the theorem for the special case of an open quantum system coupled to a single thermal reservoir. In this situation, we expect that the canonical equilibrium state $\rho^{\mathrm{eq}}[\beta]$ is the unique steady state of the system. To prove this fact, we introduce the norm [6]

$$\|\rho\|_\beta^2 = \mathrm{tr}\left[\exp[\beta H]\,\rho^\dagger \rho\right] \tag{2.25}$$

and calculate the derivative

$$\partial_t \|\rho_t\|_\beta^2 = -2\sum\nolimits_\mu \gamma^\mu \left\| [V^\mu, \exp[\beta H]\,\rho_t] \right\|_\beta^2. \tag{2.26}$$

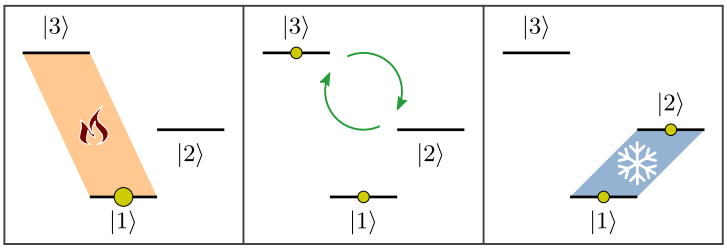

Figure 2.3. Control protocol of the cyclic 3-level maser. The three panels correspond to the three strokes, which are applied periodically. In the first stroke, the states $|1\rangle$ and $|3\rangle$ thermalize at a high temperature T_h. In the second stroke, the populations of states $|2\rangle$ and $|3\rangle$ are swapped by a π pulse. In the third stroke, the states $|1\rangle$ and $|2\rangle$ thermalize at a low temperature T_c. The yellow circles illustrate the populations of the corresponding states at the beginning of each stroke in the limit cycle. The populations are shown in the limit of large thermalization times, large hot temperature T_h and small cold temperature T_c.

This norm is therefore strictly decreasing at all times, except if the operator $\exp[\beta H]\rho_t$ commutes with all Lindblad operators, that is, if $\rho_t = \rho^{\mathrm{eq}}[\beta]$. The norm is therefore a Lyapunov function proving the convergence of any initial state to the thermal equilibrium state.

In Publication I, we extend Spohn's result to periodically driven open quantum systems, where the Lindblad generator satisfies $\hat{L}_{t+\bar{T}} = \hat{L}_t$ and $\bar{T}$ is the cycle time of the driving. In the study of periodically driven open systems, it is common to assume that they are relaxing and that their state at long times is given by a limit cycle ρ_t^{cyc} with

$$\rho_{t+\bar{T}}^{\mathrm{cyc}} = \rho_t^{\mathrm{cyc}}; \tag{2.27}$$

some examples can be found in Refs. [65–69]. We put this assumption on solid footing by showing that relaxation is certain if the generator $\hat{L}_t$ satisfies Spohn's conditions during an arbitrarily short (but finite) fraction of the cycle time. We note that this result has implications for the design of dissipative discrete time crystals [70, 71], see Publication I for details.

The proof of our theorem proceeds in three steps, which we summarize here. First, we observe that that the convergence to the limit cycle can be more easily treated in the Heisenberg picture, where the system state remains constant and the observables X carry the time dependence. The time evolution of the observables ensures that the Heisenberg picture expectation values $\mathrm{tr}\left[\rho_0 X_t\right]$ agree with the Schrödinger picture expression $\mathrm{tr}\left[\rho_t X\right]$. Hence, in the Heisenberg picture, relaxation translates to the condition that any observable X_t becomes proportional to the identity at long times. Second, we define a Lyapunov function that is strictly decreasing whenever Spohn's condition is satisfied, except if X_t is a multiple of the identity. The existence of this Lyapunov function proves that the system is relaxing. Third, a short calculation shows that the unique long-time limit cycle indeed satisfies the condition (2.27), completing our proof.

To conclude this section, we shortly discuss possible extensions of our result. It is instructive to study the cyclic 3-level maser as an example [30, 72, 73]. The 3-level maser is a 3-state quantum system, which is operated with the

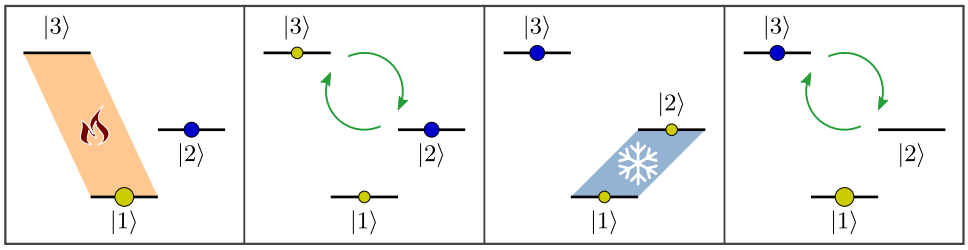

Figure 2.4. Cyclic 4-stroke protocol that does not have a unique limit cycle. The first three strokes of this protocol are identical to those of the 3-level maser shown in Fig. 2.3. In the fourth stroke, the populations of states $|2\rangle$ and $|3\rangle$ are swapped again. The ratio between the populations marked in yellow and the population marked in blue never changes, the limit cycle is therefore not unique. Figure adapted from Publication I.

control protocol shown in Fig. 2.3. Assuming that the thermalization steps are sufficiently long and the respective states thermalize completely in each step, the populations $p_t^n = \langle n|\rho_t|n\rangle$ of the levels change as follows over one driving period:

$$p_{\bar{T}}^1 = \frac{p_0^1 + p_0^3}{1+\exp[-\beta_c \varepsilon_{21}]}, \quad p_{\bar{T}}^2 = \frac{p_0^1 + p_0^3}{1+\exp[+\beta_c \varepsilon_{21}]} \quad \text{and} \quad p_{\bar{T}}^3 = p_0^2. \tag{2.28}$$

Here, p_0^n ($p_{\bar{T}}^n$) are the populations at the beginning (end) of the driving period, β_c the inverse temperature of the cold reservoir and ε_{21} the level splitting between the states $|1\rangle$ and $|2\rangle$. Even though the system does not satisfy Spohn's conditions at any time, we find that the map (2.28) has a unique fixed point. Repeated application brings the system to a unique limit cycle with populations

$$p_0^{1,\mathrm{cyc}} = \frac{\exp[\beta_c \varepsilon_{21}]}{2+\exp[\beta_c \varepsilon_{21}]} \quad \text{and} \quad p_0^{2,\mathrm{cyc}} = p_0^{3,\mathrm{cyc}} = \frac{1}{2+\exp[\beta_c \varepsilon_{21}]}. \tag{2.29}$$

We might thus conjecture that it is sufficient for the dissipative terms to connect all states of the system over the course of one period, not necessarily at the same time. However, this conjecture is false: Fig. 2.4 shows that a slight modification of the maser protocol leads to a system that is not relaxing. The formulation of a generalized relaxation criterion encompassing the cyclic 3-level maser thus requires further research. Such a criterion will have to take the unitary dynamics into account, which does not play any role in Spohn's condition.

2.5 The Semi-Classical Regime

A Lindblad equation with a Hamiltonian that commutes with itself at different times, i.e.,

$$[H_{t_1}, H_{t_2}] = 0 \tag{2.30}$$

for any two times t_1 and t_2, is referred to as semi-classical. In terms of the control operations introduced in Sec. 2.3, this condition corresponds to the exclusion of coherent driving. We introduce the projection superoperator

$$\hat{\Pi} \bullet = \sum_n |n\rangle\langle n| \bullet |n\rangle\langle n|, \tag{2.31}$$

which sets the off-diagonal elements of the state operator to zero. Here, the basis $|n\rangle$ diagonalizes the Hamiltonian at all times, and we assume for simplicity that the spectrum of the Hamiltonian is non-degenerate. Using the detailed balance condition (2.13), we find that the superoperators $\hat{\Pi}$ and $\hat{L}_t$ commute. If a semi-classical system has a unique limit cycle, it must therefore be diagonal, $[H_t, \rho_t^{\mathrm{cyc}}] = 0$.

The long-time dynamics of the system state then reduces to the dynamics of its populations, which form a probability vector with entries $p_t^n = \langle n|\rho_t|n\rangle$. This vector follows the classical master equation

$$\dot{p}_t^n = \sum\nolimits_m R_t^{nm}\, p_t^m, \tag{2.32}$$

where R_t is a rate matrix with $\sum_n R_t^{nm} = 0$ for all columns m. For $m \neq n$, the entry R_t^{nm} is the jump rate from the state m into the state n. The detailed balance property of the Lindblad equation translates to the condition

$$R_t^{nm}/R_t^{mn} = \exp\left[\beta_t\, \varepsilon_t^{mn}\right], \tag{2.33}$$

on the jump rates, where ε_t^{mn} is the energy released into the environment in a jump from m to n.

Equations of the form (2.32) are widely used in the study of classical non-equilibrium physics. They provide models for systems that can be effectively described in terms of a set of classical macrostates, like for example in biophysical processes [74] or in electronic nanostructures in the Coulomb blockade regime [75]. The transition probabilities of these models can only depend on the current macrostate and not on the history of the time evolution; the dynamics thus describes a continuous Markov process. This framework also includes diffusion processes, since the spatial discretization of Fokker-Planck equations leads to classical master equations.

We note that any classical master equation can be mapped to the population dynamics of a semi-classical Lindblad equation. Our results in Publication I therefore apply to classical master equations as well.

3. Quantum Transport

3.1 Quantum Jumps

The eponymous difference between quantum and classical physics is that quantum observables are often restricted to a discrete set of possible values; they are quantized. This phenomenon also occurs in the interaction of an open quantum system with its environment: rather than exchanging heat continuously with the reservoir, the system emits and absorbs quantized packets of energy, often in the form of photons or phonons. These emission and absorption events are accompanied by quantum jumps, abrupt changes of the system state.

In 2013, Pekola *et al.* proposed a method to experimentally detect single quantum jumps in setups based on superconducting circuits [76, 77]. In their approach, the reservoir is itself a mesoscopic object that is embedded in a macroscopic substrate, see Fig. 3.1(a). This configuration allows the reservoir to play a two-fold role. On the one hand, since it has up to ten orders of magnitude more degrees of freedom, it acts as a practically infinite thermal environment for the small system [78]. After a perturbation, it quickly returns to the equilibrium state with the substrate temperature T due to interactions with the substrate phonons. Since the characteristic time scale of this equilibration process is $\tau_E \sim 10^2\,\mathrm{ns}$ and typical relaxation times of superconducting qubits are on the order of $\bar{\tau} \sim 10^5\,\mathrm{ns}$, the Markov condition (2.10) is satisfied [79, 80]. On the other hand, the reservoir has a finite heat capacity C and can therefore function as a calorimeter. After the absorption of a photon with energy $\hbar\omega$, the reservoir temporarily reaches a thermal distribution corresponding to the temperature $T^* = T + \hbar\omega/C$. This internal thermalization takes place within nanoseconds and can thus in principle be detected before the reservoir equilibrates with the substrate again [79, 80], see Fig. 3.1(b). As the precision of modern thermometers is coming close to the required accuracy, this detection scheme might soon be realized in the lab [81–83].

Since absorption and emission events can be clearly distinguished in the time traces T_t^*, see Fig. 3.1(b), it becomes possible to implement bidirectional photon

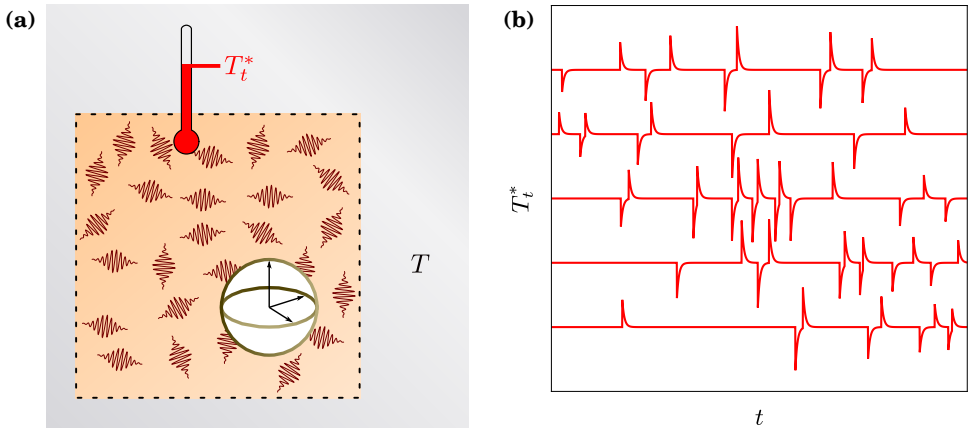

Figure 3.1. Detection of quantum jumps. (a) The setup consists of an open quantum system and a mesoscopic reservoir embedded in a substrate (gray). The temperature T of the substrate changes only slowly (time scale τ_D) and can be viewed as constant for the purpose of this discussion. The fluctuating temperature T_t^* of the reservoir is monitored accurately. (b) The plot shows five idealized examples of time traces T_t^*. An upward spike indicates the absorption of a photon in the reservoir at the respective time. The height of the spike corresponds to the energy carried by the photon. Similarly, downward spikes correspond to emitted photons. After each event, T_t^* quickly returns to the background temperature T. Figure (b) adapted from Publication IV.

counting. The ability to observe single quantum jumps thus opens the door for the investigation of new types of statistical properties of quantum transport processes. As we will discuss in Chapter 4, the framework also enables us to analyze thermodynamic quantities and their fluctuations [9, 84–86].

In order to describe the statistics of quantum jumps quantitatively, we now express the dynamics of the Lindblad equation as an average of quantum jump trajectories, weighted with their probabilities. This procedure, called the unraveling of the Lindblad master equation, is comparable to the path integral formulation of classical stochastic dynamics, where a diffusive process is expressed as an average over stochastic trajectories following Langevin dynamics [87]. Like a trajectory in stochastic dynamics, a quantum jump trajectory corresponds to a single realization of the experiment. It describes the time evolution of a pure state $|\psi_\tau\rangle\langle\psi_\tau|$, which is continuous and deterministic except for a number of quantum jumps [1, 88]. Along the continuous parts of the trajectory, the state follows the von Neumann equation

$$\partial_\tau|\psi_\tau\rangle\langle\psi_\tau| = \frac{1}{\mathrm{i}\hbar}\left(H_\tau^{\mathrm{eff}} - \left\langle H_\tau^{\mathrm{eff}}\right\rangle\right)|\psi_\tau\rangle\langle\psi_\tau| - \frac{1}{\mathrm{i}\hbar}|\psi_\tau\rangle\langle\psi_\tau|\left(H_\tau^{\mathrm{eff}} - \left\langle H_\tau^{\mathrm{eff}}\right\rangle\right)^\dagger, \tag{3.1}$$

where $\langle\bullet\rangle = \langle\psi_\tau|\bullet|\psi_\tau\rangle$ signifies the expectation value and

$$H_\tau^{\mathrm{eff}} = H_\tau - \frac{\mathrm{i}\hbar}{2}\sum\nolimits_\mu \gamma_\tau^\mu V_\tau^{\mu\dagger} V_\tau^\mu \tag{3.2}$$

is the effective, non-Hermitian Hamiltonian. These continuous trajectories are interrupted by stochastic quantum jumps, each associated with a specific dissipation channel of the Lindblad generator. The probability for the channel μ to induce a jump during the infinitesimal time interval $[\tau, \tau + \mathrm{d}\tau]$ is given by

$$\mathrm{d}P_\tau^\mu = \gamma_\tau^\mu \left\langle V_\tau^{\mu\dagger} V_\tau^\mu \right\rangle \mathrm{d}\tau, \tag{3.3}$$

and the state of the system after the jump is

$$V_\tau^\mu |\psi_\tau\rangle\langle\psi_\tau| V_\tau^{\mu\dagger} \,/\, \left\langle V_\tau^{\mu\dagger} V_\tau^\mu \right\rangle. \tag{3.4}$$

A jump trajectory $\mathbb{T}$ is fully specified by its initial state $|\psi_0\rangle\langle\psi_0|$, the times t_k of the jumps and the corresponding channels μ_k. For a fixed initial state, the probability $\mathbb{P}$ of a jump trajectory is given by the product of the jump probabilities (3.3) and the probability of no jumps occurring at any other time, i.e.,

$$\mathbb{P}[\mathbb{T}|\psi_0] = \exp\left[-\int_0^t \left(\sum\nolimits_\mu \frac{\mathrm{d}P_\tau^\mu}{\mathrm{d}\tau}\right) \mathrm{d}\tau\right] \prod\nolimits_{k=1}^N \frac{\mathrm{d}P_{t_k}^\mu}{\mathrm{d}t_k}. \tag{3.5}$$

Here, t is the total duration of the process and N is the number of jumps on the trajectory $\mathbb{T}$. The probabilities $\mathrm{d}P_\tau^\mu$ are evaluated along the trajectory and $\mathrm{d}P_{t_k}^\mu$ is evaluated in the state before the jump.

In order to reconstruct the time evolution of the state operator from the quantum jump trajectories, we assume that the system is initially in the mixed state

$$\rho_0 = \sum\nolimits_n r_0^n |\psi_0^n\rangle\langle\psi_0^n|. \tag{3.6}$$

The state at the time t can then be obtained from the weighted average of the final states of the trajectories,

$$\rho_t = \sum\nolimits_n r_0^n \int_0^t \mathrm{d}\mathbb{T}\, \mathbb{P}[\mathbb{T}|\psi_0^n]\, |\psi_t[\mathbb{T}]\rangle\langle\psi_t[\mathbb{T}]|. \tag{3.7}$$

Here, the path integral $\int_0^t \mathrm{d}\mathbb{T}$ sums over all trajectories and is formally defined as

$$\int_0^t \mathrm{d}\mathbb{T} = \sum\nolimits_{N=0}^\infty \int_0^t \mathrm{d}t_1 \sum\nolimits_{\mu_1} \int_{t_1}^t \mathrm{d}t_2 \sum\nolimits_{\mu_2} \cdots \int_{t_{N-1}}^t \mathrm{d}t_N \sum\nolimits_{\mu_N}. \tag{3.8}$$

Using Eq. (3.5), it can be verified that the expression (3.7) satisfies the original Lindblad equation.

3.2 Statistics of Counting Variables

Given a quantum jump trajectory, i.e., a record of jump times t_k and corresponding channels μ_k, it is natural to identify the net amount of energy transferred from the environment to the system as

$$Q[\mathbb{T}] = \sum\nolimits_{k=1}^N \varepsilon_{t_k}^{\mu_k}. \tag{3.9}$$

The random variable Q thus counts the amount of transferred energy by summing up the photon energies of the individual jump events. In general, we refer to a random variable X as a counting variable if X increases or decreases at every jump event by a prescribed increment x_t^μ.

In the following, we determine the full counting statistics of X, that is, its distribution over many realizations of the experiment, each corresponding to

a different quantum jump record. To this end, we modify the quantum jump trajectories, adding a phase that keeps track of the accumulated counter along the trajectory. On the continuous parts of the trajectory, this phase remains constant. The jump prescription (3.4) is modified so that the phase is incremented by χx_τ^μ at a jump,

$$\mathrm{e}^{\mathrm{i}\chi X_\tau}|\psi_\tau\rangle\langle\psi_\tau| \quad\to\quad \mathrm{e}^{\mathrm{i}\chi(X_\tau+x_\tau^\mu)}V_\tau^\mu|\psi_\tau\rangle\langle\psi_\tau|V_\tau^{\mu\dagger}\,/\,\big\langle V_\tau^{\mu\dagger}V_\tau^\mu\big\rangle, \tag{3.10}$$

where χ is an auxiliary variable, the counting field [89–91]. Taking the weighted average

$$\rho_t(\chi)=\sum\nolimits_n r_0^n\int_0^t \mathrm{d}\mathbb{T}\,\mathbb{P}[\mathbb{T}|\psi_0^n]\,\mathrm{e}^{\mathrm{i}\chi X_t[\mathbb{T}]}|\psi_t[\mathbb{T}]\rangle\langle\psi_t[\mathbb{T}]| \tag{3.11}$$

yields a χ-dependent, non-Hermitian state operator, which follows the modified Lindblad equation $\dot\rho_t(\chi)=\hat L_t(\chi)\rho_t(\chi)$ with

$$\hat L_t(\chi)\bullet=\frac{1}{\mathrm{i}\hbar}[H_t,\bullet]+\sum\nolimits_\mu\gamma_t^\mu\left(\mathrm{e}^{\mathrm{i}\chi x_t^\mu}V_t^\mu\bullet V_t^{\mu\dagger}-\frac{1}{2}\Big\{V_t^{\mu\dagger}V_t^\mu,\bullet\Big\}\right). \tag{3.12}$$

After solving the modified Lindblad equation, the full counting statistics of X can be obtained by taking the Fourier transform,

$$P_t[X]=\sum\nolimits_n r_0^n\int_0^t \mathrm{d}\mathbb{T}\,\mathbb{P}[\mathbb{T}|\psi_0^n]\,\delta\big[X-X_t[\mathbb{T}]\big]=\frac{1}{2\pi}\,\mathrm{tr}\int_{-\infty}^{\infty}\rho_t(\chi)\mathrm{e}^{-\mathrm{i}\chi X}\,\mathrm{d}\chi. \tag{3.13}$$

This distribution is characterized by its moment-generating function

$$\mathscr{M}_t(\chi)=\int_{-\infty}^{\infty}P_t[X]\mathrm{e}^{\mathrm{i}\chi X}\,\mathrm{d}X=\mathrm{tr}\,\rho_t(\chi) \tag{3.14}$$

and cumulant-generating function

$$\mathscr{K}_t(\chi)=\log\mathscr{M}_t(\chi), \tag{3.15}$$

from which all moments and cumulants can be derived,

$$\langle X^n\rangle_t=\big(-\mathrm{i}\partial_\chi\big)^n\mathscr{M}_t(\chi)\big|_{\chi=0}\quad\text{and}\quad\langle\langle X^n\rangle\rangle_t=\big(-\mathrm{i}\partial_\chi\big)^n\mathscr{K}_t(\chi)\big|_{\chi=0}. \tag{3.16}$$

The first and second cumulant are the mean $\langle\langle X\rangle\rangle_t=\langle X\rangle_t$ and the variance $\langle\langle X^2\rangle\rangle_t=\langle X^2\rangle_t-\langle X\rangle_t^2$ of the distribution. In non-critical systems, all cumulants grow linearly at long times [92, 93]. It is convenient to define the rescaled cumulant-generating function

$$\bar{\mathscr{K}}(\chi)=\lim_{t\to\infty}\frac{1}{t}\mathscr{K}_t(\chi), \tag{3.17}$$

which, in time-homogeneous systems, is equal to the eigenvalue of $\hat L(\chi)$ with the largest real part [91].

Using the methods introduced here, we now determine the average rate of quantum jumps. To this end, we consider the variable N^μ which counts the number of jumps in the dissipation channel μ. In the event of a quantum jump

in the channel ν, this variable increases by the amount $(n^\mu)_t^\nu = \delta^{\mu\nu}$. The average jump rate in channel μ is thus given by

$$j_t^\mu = \partial_t \langle N^\mu \rangle_t = -\mathrm{i}\,\partial_\chi \,\mathrm{tr}\left[\partial_t \rho_t(\chi)\right]\Big|_{\chi=0} = \gamma_t^\mu \,\mathrm{tr}\left[V_t^\mu \rho_t V_t^{\mu\dagger}\right]. \tag{3.18}$$

The mean value of any counting variable can be expressed in terms of the jump rates j_t^μ as follows:

$$\langle X \rangle_t = \int_0^t \partial_\tau \langle X \rangle_\tau \,\mathrm{d}\tau = \int_0^t \left(\sum\nolimits_\mu x_\tau^\mu j_\tau^\mu\right) \mathrm{d}\tau. \tag{3.19}$$

3.3 Full Counting Statistics of the Quantum Harmonic Oscillator

Next to the damped qubit introduced in Sec. 2.3, the damped quantum harmonic oscillator is possibly the most important model of an open quantum system [1]. Its state operator follows the Lindblad equation

$$\begin{aligned}\dot\rho_t = -\mathrm{i}\omega[a^\dagger a, \rho_t] + \gamma(\bar n + 1)\left(a\rho_t a^\dagger - \frac{1}{2}\{a^\dagger a, \rho_t\}\right) \\ + \gamma \bar n \left(a^\dagger \rho_t a - \frac{1}{2}\{a a^\dagger, \rho_t\}\right),\end{aligned} \tag{3.20}$$

where a and $a^\dagger$ are the ladder operators of the harmonic oscillator and $\hbar\omega$ its level splitting. Further, γ is the characteristic rate of photon emissions and absorptions and $\bar n = (\exp[\hbar\omega\beta] - 1)^{-1}$ the Bose-Einstein factor, i.e., the mean number of excitations in the system in equilibrium. Equation (3.20) describes, for example, the damping of a light mode in a microwave cavity due to the interaction with modes outside the cavity. The microwave photons that are exchanged in this interaction can be detected, e.g., using the scheme introduced in Sec. 3.1 or using Josephson junctions [94]. In Publication II, we analytically derive the full counting statistics of these photons and find that this model, despite its apparent simplicity, is very rich in physics.

In this overview, we focus on the emission statistics of the cavity, which only considers the outgoing photons and ignores the incoming ones. In order to derive the moment-generating function, we introduce a counting field in the Lindblad equation and obtain

$$\begin{aligned}\dot\rho_t(\chi) = -\mathrm{i}\omega[a^\dagger a, \rho_t(\chi)] + \gamma(\bar n + 1)\left(\mathrm{e}^{\mathrm{i}\chi} a\rho_t(\chi)a^\dagger - \frac{1}{2}\{a^\dagger a, \rho_t(\chi)\}\right) \\ + \gamma \bar n \left(a^\dagger \rho_t(\chi) a - \frac{1}{2}\{a a^\dagger, \rho_t(\chi)\}\right).\end{aligned} \tag{3.21}$$

The population dynamics of this equation can be solved analytically, resulting in the explicit expression

$$\mathscr{M}_t(\chi) = \mathscr{G}\left[\log\left(\frac{2\bar n + 1}{2\bar n} - \frac{\xi}{2\bar n}\frac{\xi\sinh\left[\frac{\xi\gamma t}{2}\right] + \cosh\left[\frac{\xi\gamma t}{2}\right]}{\xi\cosh\left[\frac{\xi\gamma t}{2}\right] + \sinh\left[\frac{\xi\gamma t}{2}\right]}\right)\right] \frac{\xi\,\mathrm{e}^{\gamma t/2}}{\xi\cosh\left[\frac{\xi\gamma t}{2}\right] + \sinh\left[\frac{\xi\gamma t}{2}\right]} \tag{3.22}$$

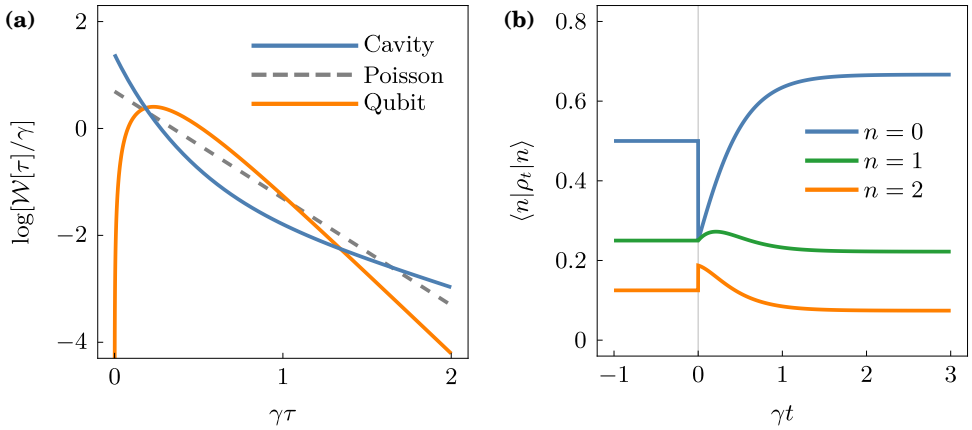

Figure 3.2. Emission statistics of a microwave cavity. (a) Comparison of the waiting time distribution of the cavity emission current with that of a Poisson emitter with the same average emission rate, and with that of a qubit with the same temperature and the same average emission rate. Note that the waiting time distribution of a Poisson process is an exponential distribution. (b) Populations of the lowest three energy levels. The system is initially ($t < 0$) in thermal equilibrium and a photon is emitted at time $t = 0$. For times $t > 0$, the plot shows the conditional populations assuming that no additional emission event happens. Both figures are adapted from Publication II. The temperature was chosen so that the mean number of cavity excitations is $\bar{n} = 1$.

for the moment-generating function [PII]. Here, $\xi = \sqrt{1 - 4\bar{n}(1+\bar{n})(e^{i\chi} - 1)}$ and $\mathcal{G}$ is the Laplace transform of the initial populations,

$$\mathcal{G}[q] = \sum_{n=0}^{\infty} \langle n|\rho_0|n\rangle \, e^{nq}. \tag{3.23}$$

If the system is initially in the thermal equilibrium state $\rho^{\mathrm{eq}}[\beta]$, the moment-generating function simplifies to

$$\mathcal{M}_t(\chi) = \frac{2\xi \, e^{\gamma t/2}}{2\xi \cosh\left[\frac{\xi\gamma t}{2}\right] + (1+\xi^2)\sinh\left[\frac{\xi\gamma t}{2}\right]}. \tag{3.24}$$

As a first application of this result, we calculate the average emission rate in equilibrium and find

$$\partial_t \langle N^{\downarrow}\rangle_t = -i\partial_t \partial_\chi \mathcal{M}_t(\chi)\big|_{\chi=0} = \gamma\bar{n}(\bar{n}+1), \tag{3.25}$$

which agrees with the expression $j_t^{\downarrow} = \gamma(\bar{n}+1)\,\mathrm{tr}\left[a\rho^{\mathrm{eq}}a^\dagger\right]$ derived in Sec. 3.2. Here, the index $\downarrow$ stands for the emission channel with Lindblad operator $V^{\downarrow} = a$.

As another application of our results, we analyze the waiting time distribution of the emitted photons, i.e., the probability distribution $\mathcal{W}[\tau]$ of the times τ between two subsequent events. Waiting time distributions provide a powerful tool for the analysis of counting experiments [95–98]; they can be derived from the moment-generating function using the formula [99, 100]

$$\mathcal{W}[\tau] = c\,\partial_\tau^2 \mathcal{M}_\tau(\chi = i\infty), \tag{3.26}$$

where the constant c is fixed by the normalization condition $\int_0^\infty \mathcal{W}[\tau]\,d\tau = 1$. In Fig. 3.2(a), we compare the waiting time distribution of the cavity emission

current with that of a Poisson process, i.e., a process where all emission events are statistically independent. We find that both the probability of short waiting times and the probability of long waiting times are enhanced in the cavity. The emitted photons therefore exhibit a bunching effect, where series of multiple events in rapid succession are separated by long idle times, indicating the bosonic nature of the cavity. To study this effect further, we used Bayes' theorem to calculate how the populations of the cavity change at an emission event. The results, which are plotted in Fig. 3.2(b), show that the probability of zero photons immediately decreases and the populations of higher-energy states increase. This behavior is unintuitive from a classical point of view, but it is required in order to explain photon bunching. We refer to Publication II for a more quantitative investigation of this effect and the discussion of further properties of the cavity photon statistics.

It is instructive to compare our results to the emission statistics of the damped qubit. To derive its emission statistics, we introduce a counting field in the qubit master equation, which becomes

$$\dot{\rho}_t(\chi) = \mathrm{i}\omega[\sigma_z, \rho_t(\chi)] + \gamma(1-\bar{n}_\mathrm{F})\left(\mathrm{e}^{\mathrm{i}\chi}\sigma^\downarrow\rho_t(\chi)\sigma^\uparrow - \frac{1}{2}\{\sigma^\uparrow\sigma^\downarrow, \rho_t(\chi)\}\right) + \gamma\bar{n}_\mathrm{F}\left(\sigma^\uparrow\rho_t(\chi)\sigma^\downarrow - \frac{1}{2}\{\sigma^\downarrow\sigma^\uparrow, \rho_t(\chi)\}\right). \tag{3.27}$$

We here parametrized the coupling rates in terms of the Fermi-Dirac factor $\bar{n}_\mathrm{F} = (\exp[\hbar\omega\beta]+1)^{-1}$ and rescaled the rate γ by a factor $\bar{n}/\bar{n}_\mathrm{F}$ compared with Eq. (2.19). The moment-generating function is derived in a straightforward way; it is given by

$$\mathscr{M}_t(\chi) = \frac{2\xi_\mathrm{F}\cosh\left[\frac{\xi_\mathrm{F}\gamma t}{2}\right] + (1+\xi_\mathrm{F}^2)\sinh\left[\frac{\xi_\mathrm{F}\gamma t}{2}\right]}{2\xi_\mathrm{F}\,\mathrm{e}^{\gamma t/2}}, \tag{3.28}$$

in thermal equilibrium [101], where $\xi_\mathrm{F} = \sqrt{1+4\bar{n}_\mathrm{F}(1-\bar{n}_\mathrm{F})(\mathrm{e}^{\mathrm{i}\chi}-1)}$. The photons emitted from the qubit exhibit an anti-bunching behavior, which is characteristic for fermionic systems, see Fig. 3.2(a). We observe that the moment-generating functions (3.24) and (3.28) are related by the symmetry transformation

$$\mathscr{M}_\mathrm{fermion} = \left(\mathscr{M}_\mathrm{boson}\right)^{-1}_{\bar{n}\to-\bar{n}_\mathrm{F}}. \tag{3.29}$$

A similar relation holds for the statistics of ballistic transport of non-interacting particles between fermionic or bosonic leads [102]. The question whether this correspondence can be generalized is an interesting opportunity for future research.

3.4 First Passage Time Distributions

The study of counting variables in stochastic processes is often motivated by the question how long it will take the counter to hit a certain threshold. This threshold could, for example, correspond to the win or loss of a game, to the

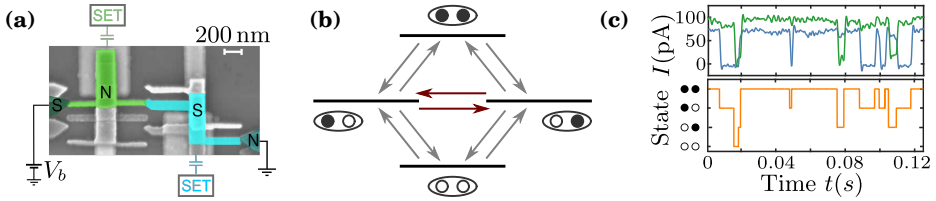

Figure 3.3. Electronic states of a double quantum dot. (a) Scanning electron micrograph of our setup, which consist of one normal metal (N) and one superconducting (S) metallic island forming a double quantum dot. The state of the island can be detected with the coupled single-electron transistors (SETs). A voltage bias V_b is applied to the connected leads. (b) Schematic diagram of the four charge states of the double quantum dot, where each island can have either 0 or 1 extra electron, and the possible transitions. The net charge transfer is measured by counting the transitions between the states $|\bullet\circ\rangle$ and $|\circ\bullet\rangle$. (c) The time trace of the system state (bottom panel) is inferred from the current through the single-electron transistors (top panel). All figures adapted from Publication III.

capture of a Brownian particle in a potential well, or to the bankruptcy of a financial trader [103]. The length of time from the beginning of the experiment until a threshold M is reached is a random variable called the first passage time or first hitting time. Its probability distribution distribution is the first passage time distribution $\mathscr{P}_M[t]$.

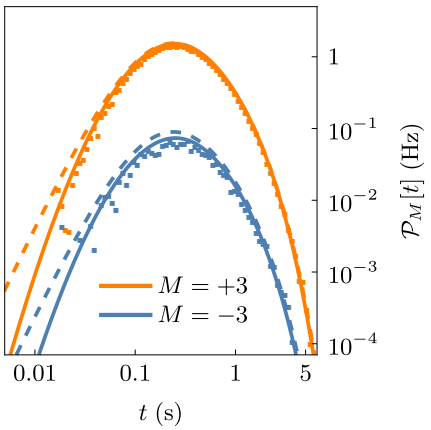

Figure 3.4. First passage time distributions of the net transferred charge with two thresholds M. The dots are directly derived from the experimental data. The solid curves correspond to the exact theory and the dashed curves to the random walk approximation. Figure adapted from Publication III.

In Publication III, we study the first passage time distribution of charge transport in an electronic nanostructure both experimentally and theoretically. Our setup, depicted in Fig. 3.3(a), consists of a double quantum dot with an applied charge bias [104]. In the Coulomb-blockade regime, each dot is either in its ground state $|\circ\rangle$ or occupied by one extra electron $|\bullet\rangle$. The configuration space of the double quantum dot thus consists of the four charge states shown in Fig. 3.3(b), which can all be distinguished in the experiment, see Fig. 3.3(c). This arrangement makes it possible to bidirectionally count the transferred electrons [105]: the total number of electrons that move from the left to the right lead corresponds to the number of transitions from $|\bullet\circ\rangle$ to $|\circ\bullet\rangle$, and vice versa. Following Publication III, we focus on the net amount N_t of transferred charge, which is given by

$$N_t = \#_t\big(|\bullet\circ\rangle \to |\circ\bullet\rangle\big) - \#_t\big(|\circ\bullet\rangle \to |\bullet\circ\rangle\big) \tag{3.30}$$

(in units of the elementary charge). Here, # denotes the number of transitions.

In Fig. 3.4, we show first passage time distributions of N_t at two different thresholds M. Due to the applied bias, the distribution with $M > 0$ is normalized, i.e., $\int_0^\infty \mathscr{P}_M[t]\, \mathrm{d}t = 1$. The distribution with $M < 0$ is not normalized since,

for some realizations, the threshold is never reached. The results in Fig. 3.4 are obtained using three different methods, which are in excellent agreement. First, we read off the first passage times directly from the experimental data by counting the transitions between the states $|\bullet\circ\rangle$ and $|\circ\bullet\rangle$ in the measured time traces. Second, we use the experimental data to estimate the average transition rates between the charge states of the double quantum dot and thus formulate a model of the system based on a classical master equation. By introducing a counting field, we obtain the moment-generating function of the net charge transfer, from which the first passage time distributions can be derived [106, 107].

The third method is based on approximating the counting process as a random walk. The inner structure of the Markov process, depicted in Fig. 3.3(b), is thus discarded. Instead, we assume that the counter N_t can increase by an amount α with the probability $R_+ \, \mathrm{d}t$ at any time, or decrease by the same amount with probability $R_- \, \mathrm{d}t$. The simplified model has the form of an asymmetric random walk, which has the rescaled cumulant-generating function [99]

$$\bar{\mathcal{K}}^{\mathrm{RW}}(\chi) = R_+ \left(\mathrm{e}^{\mathrm{i}\alpha\chi} - 1\right) + R_- \left(\mathrm{e}^{-\mathrm{i}\alpha\chi} - 1\right). \tag{3.31}$$

The three free parameters $R_\pm$ and α are chosen such that the first three rescaled cumulants $C_k = \lim_{t\to\infty} t^{-1} \langle\langle N^k \rangle\rangle_t$ of the random walk agree with those of the original process. Our approximation thereby goes beyond a Gaussian model, involving not only the mean and the variance but also the third cumulant.

We approximate $\mathscr{P}_M[t]$ with the first passage time distribution of the random walk with threshold

$$M^* = \left\lceil M/\alpha \right\rfloor = \left\lceil M\sqrt{C_1/C_3} \right\rfloor, \tag{3.32}$$

where $\lceil\bullet\rfloor$ denotes rounding. It is given by [108]

$$\mathscr{P}_M[t] \approx \mathscr{P}^{\mathrm{RW}}_{M^*}[t] = \frac{|M^*|\,\mathrm{e}^{-\frac{C_1 C_2}{C_3} t}}{t} \left(\frac{C_2 + \sqrt{C_1 C_3}}{C_2 - \sqrt{C_1 C_3}}\right)^{M^*/2} I_{|M^*|}\left[\frac{C_1\sqrt{C_2^2 - C_1 C_3}}{C_3} t\right], \tag{3.33}$$

where $I_n[x]$ is the modified Bessel function of the first kind. The distributions exhibit the fluctuation relation

$$\frac{\mathscr{P}_M[t]}{\mathscr{P}_{-M}[t]} = \left(\frac{C_2 + \sqrt{C_1 C_3}}{C_2 - \sqrt{C_1 C_3}}\right)^{M^*}, \tag{3.34}$$

which we confirmed in the experimental data.

4. Quantum Thermodynamics

4.1 The Laws of Thermodynamics

The classical theory of thermodynamics describes transformations between equilibrium states of physical ensembles, which can be characterized by a small number of macroscopic variables. It is purely based on statistical laws and does not make assumptions on the underlying microscopic dynamics. While this theory has been remarkably successful in explaining fundamental thermodynamic relations, it cannot be used to describe processes that take place far from equilibrium. To study realistic heat engines with finite power output, it is thus necessary to identify the basic thermodynamic quantities, including entropy, internal energy, work and heat, in terms of the microscopic degrees of freedom.

In the following, we introduce the standard framework of quantum thermodynamics in the weak-coupling regime [7, 20]. Here, the thermodynamic internal energy of the working system is identified with the expectation value of the system Hamiltonian,

$$U_t = \mathrm{tr}\big[H_t \rho_t\big]\,. \tag{4.1}$$

The time derivative of the internal energy can be divided into two contributions,

$$\dot{W}_t = -\,\mathrm{tr}\big[\dot{H}_t \rho_t\big] \quad \text{and} \quad \dot{Q}_t = \mathrm{tr}\big[H_t \dot{\rho}_t\big]\,. \tag{4.2}$$

The first term $\dot{W}_t$ describes the decrease of the system energy due to the external driving and is therefore identified with the power output of the device. The total work produced until the time t is $W_t = \int_0^t \dot{W}_\tau \,\mathrm{d}\tau$. The other term corresponds to the heat current from the environment into the system. Using the detailed balance condition, we can rewrite it in the form

$$\dot{Q}_t = \sum\nolimits_\mu \varepsilon_t^\mu j_t^\mu\,, \tag{4.3}$$

showing that the definition here agrees with the ensemble average of the variable $Q[\mathbb{T}]$, introduced in Sec. 3.2, which counts the transferred energy on the

trajectory level. In a multi-reservoir setup, each reservoir provides the separate contribution

$$\dot{Q}_t^m = \mathrm{tr}\left[H_t \hat{D}_t^m \rho_t\right] \tag{4.4}$$

to the total heat current, cf. Eq. (2.15). Together, these relations imply that the first law of thermodynamics holds,

$$\dot{U}_t = -\dot{W}_t + \dot{Q}_t = -\dot{W}_t + \sum\nolimits_m \dot{Q}_t^m. \tag{4.5}$$

The total entropy production rate consists of contributions from the system and the environment. The system entropy is identified with the von Neumann entropy

$$S_t = -k_\mathrm{B}\,\mathrm{tr}\left[\rho_t \log \rho_t\right] \tag{4.6}$$

and the entropy production in the reservoirs is given by the expression

$$\dot{S}_t^\mathrm{env} = -k_\mathrm{B} \sum\nolimits_m \beta_t^m \dot{Q}_t^m. \tag{4.7}$$

The total entropy production is therefore

$$\begin{aligned} \dot{S}_t^\mathrm{tot} &= \dot{S}_t + \dot{S}_t^\mathrm{env} = \sum\nolimits_m \dot{S}_t^{m,\mathrm{tot}}, \quad \text{where} \\ \dot{S}_t^{m,\mathrm{tot}} &= k_\mathrm{B}\,\mathrm{tr}\left[\left(\hat{D}_t^m \rho_t\right)\left(\log \rho_t^\mathrm{eq}[\beta_t^m] - \log \rho_t\right)\right]. \end{aligned} \tag{4.8}$$

Using the identity (2.16), it follows from a theorem by Spohn that each contribution $\dot{S}_t^{m,\mathrm{tot}}$ is non-negative [109]. Hence, the second law of thermodynamics holds at all times,

$$\dot{S}_t^\mathrm{tot} \geq 0, \tag{4.9}$$

and the adiabatic weak-coupling framework is consistent with the laws of thermodynamics.

The total entropy production is a measure for the irreversibility of a process and thus related to its thermodynamic cost [110]. In order to quantify the origin of this cost, it is useful to divide the total entropy production into multiple parts, each of which is non-negative. For example, in Publication IV, we propose to split the entropy production into one contribution stemming from the quantum jumps and one stemming from the decay of superpositions,

$$\dot{S}_t^{m,\mathrm{tot}} = \dot{S}_t^{m,\mathrm{j}} + \dot{S}_t^{m,\mathrm{coh}}. \tag{4.10}$$

The first contribution is given by

$$\dot{S}_t^{m,\mathrm{j}} = \frac{k_\mathrm{B}}{2} \sum\nolimits_\mu^{(m)} \left(j_t^\mu - j_t^{\mu\dagger}\right) \log\left[j_t^\mu / j_t^{\mu\dagger}\right] \geq 0, \tag{4.11}$$

where the sum $\sum_\mu^{(m)}$ runs over all dissipation channels associated with the m-th reservoir. This expression agrees with the standard definition of the total entropy production rate in Markov jump processes [74]. The remaining $\dot{S}_t^{m,\mathrm{coh}} = (\dot{S}_t^{m,\mathrm{tot}} - \dot{S}_t^{m,\mathrm{j}})$ is separately non-negative and can thus be understood as a measure for the thermodynamic cost of coherence [PIV].

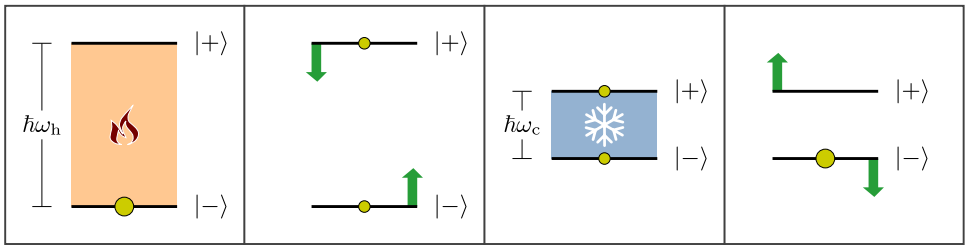

Figure 4.1. Control protocol of the quantum Otto engine based on a qubit. The four panels correspond to the four strokes, explained in the main text, which are applied periodically. The horizontal lines represent the states of the qubit and their distance represents the level splitting at the beginning of each stroke. The yellow circles illustrate the populations of the corresponding states at the beginning of each stroke in the limit cycle. The populations are shown in the limit of large thermalization times, large hot temperature T_h and small cold temperature T_c.

Another way to split the total entropy production into multiple parts has been put forward by Polkovnikov in form of the diagonal entropy production rate [111]

$$\dot{S}_t^{m,\mathrm{d}} = k_\mathrm{B}\,\mathrm{tr}\big[\big(\hat{D}_t^m \hat{\Pi}_t \rho_t\big)\big(\log\rho_t^{\mathrm{eq}}[\beta_t^m] - \log\hat{\Pi}_t\rho_t\big)\big] \geq 0. \tag{4.12}$$

Recall that the superoperator $\hat{\Pi}_t$ projects the state ρ_t to the diagonal in the instantaneous energy eigenbasis. Both $\dot{S}_t^{m,\mathrm{d}}$ and its complement $(\dot{S}_t^{m,\mathrm{tot}} - \dot{S}_t^{m,\mathrm{d}})$ are non-negative [36, 112]. In fact, the diagonal entropy production $\dot{S}_t^{m,\mathrm{d}}$ and the jump entropy production $\dot{S}_t^{m,\mathrm{j}}$ are closely related: a straightforward extension of our argument in Publication IV shows that they form the hierarchy

$$\dot{S}_t^{m,\mathrm{tot}} \geq \dot{S}_t^{m,\mathrm{d}} \geq \dot{S}_t^{m,\mathrm{j}} \geq 0 \tag{4.13}$$

and that they are equal if all Lindblad operators are simple jumps. The term simple jump refers to a Lindblad operator with the form $V_t^\mu = |n_t\rangle\langle m_t|$, where $|n_t\rangle$ and $|m_t\rangle$ are instantaneous energy eigenstates.

4.2 Thermal Machines

Thermal machines are devices that convert heat and other forms of energy into each other. They can be classified into two categories [21, 32, 113]: continuous devices that operate in a non-equilibrium steady state, like for example thermoelectric generators [114, 115], and cyclic or reciprocating devices that are subject to external time-periodic control [60, 116]. Since coherence can only be maintained by time-dependent external driving in the adiabatic weak-coupling regime, we here focus on cyclic devices. They generally consist of a working fluid which is either coupled to one reservoir with periodically modulated temperature, or in alternation to two reservoirs with constant temperatures [117].

The quantum Otto engine is a paradigmatic example of a cyclic quantum heat engine [67, 116, 118–122]. Its control protocol consists of two isentropic and two isochoric strokes as shown in Fig. 4.1. In the isentropic strokes, the system is decoupled from the reservoirs and performs work. In the isochoric strokes, heat is transferred between the system and the hot or the cold reservoir without

changing the external parameters. For a quantitative discussion, we consider a single qubit Otto engine with a Hamiltonian of the form

$$H_t = \frac{\hbar\Delta}{2}\sigma_x + \frac{\hbar\sqrt{\omega_t^2 - \Delta^2}}{2}\sigma_z, \tag{4.14}$$

where $\hbar\omega_t$ is the level splitting of the qubit, $\hbar\Delta$ the tunneling energy and $\hbar\sqrt{\omega_t^2 - \Delta^2}$ the tunable energy bias [123]. In the following, we analyze each stroke of the Otto cycle in detail. We focus first on the semi-classical regime with $\Delta = 0$, where the system state is fully described by the z-component of the Bloch vector, z_t.

Stroke 1 (Isochoric). During the first stroke, the qubit thermalizes with the hot reservoir for the duration t_h and the level splitting ω_h is kept constant. The state evolves according to the Bloch equation

$$\dot{z}_t = -\gamma(1 + 2\bar{n}_\mathrm{h})z_t - \gamma \tag{4.15}$$

with the Bose-Einstein factor $\bar{n}_\mathrm{h} = (\exp[\hbar\omega_\mathrm{h}\beta_\mathrm{h}] - 1)^{-1}$, the inverse reservoir temperature β_h and the coupling rate γ. After this stroke, the system state is given by

$$z_{(1)} = \frac{1 + z_{(0)}(1 + 2\bar{n}_\mathrm{h})}{1 + 2\bar{n}_\mathrm{h}} \mathrm{e}^{-\gamma(1+2\bar{n}_\mathrm{h})t_\mathrm{h}} - \frac{1}{1 + 2\bar{n}_\mathrm{h}}, \tag{4.16}$$

where $z_{(k)}$ denotes the state after the k-th stroke and $z_{(0)}$ the initial state. During the stroke, the system absorbs the heat $Q_\mathrm{in} = U_{(1)} - U_{(0)} = \hbar\omega_\mathrm{h}(z_{(1)} - z_{(0)})$, which plays the role of the engine input.

Stroke 2 (Isentropic). In the second stroke, the level splitting is reduced to $\omega_\mathrm{c} < \omega_\mathrm{h}$. Because the reservoirs are decoupled, the system state does not change, i.e., $z_{(2)} = z_{(1)}$. This step has the energy cost $W_\mathrm{in} = U_{(2)} - U_{(1)} = \hbar(\omega_\mathrm{c} - \omega_\mathrm{h})z_{(2)}$.

Stroke 3 (Isochoric). Here, the qubit thermalizes with the cold reservoir for the duration t_c and the level splitting ω_c is kept constant. In the process, the engine deposits the waste heat $Q_\mathrm{out} = \hbar\omega_\mathrm{c}(z_{(2)} - z_{(3)})$ into the reservoir. The final state $z_{(3)}$ can be determined in analogy to the first stroke.

Stroke 4 (Isentropic). In the final stroke, the level splitting returns to its original value ω_h. The state remains constant, $z_{(4)} = z_{(3)}$, and the system is able to perform the work $W_\mathrm{out} = \hbar(\omega_\mathrm{c} - \omega_\mathrm{h})z_{(4)}$. The net work output during one operation cycle is $W = W_\mathrm{out} - W_\mathrm{in}$.

Once the system has settled in its cyclic state with $z_{(4)} = z_{(0)}$, the first and the second law take the form

$$W = Q_\mathrm{in} - Q_\mathrm{out} \qquad \text{and} \qquad \beta_\mathrm{c}Q_\mathrm{out} - \beta_\mathrm{h}Q_\mathrm{in} \geq 0, \tag{4.17}$$

and the work output is

$$W = \hbar(\omega_\mathrm{h} - \omega_\mathrm{c})\left(\tanh\left[\frac{\hbar\omega_\mathrm{c}\beta_\mathrm{c}}{2}\right] - \tanh\left[\frac{\hbar\omega_\mathrm{h}\beta_\mathrm{h}}{2}\right]\right) \tag{4.18}$$

in the limit of long thermalization times ($t_c, t_h \to \infty$). For the engine to produce positive work, the control parameters must therefore satisfy the working condition

$$\frac{T_c}{T_h} < \frac{\omega_c}{\omega_h} < 1. \tag{4.19}$$

We note that this result does not change if the thermalization times t_c and t_h are finite.

For other values of the system parameters, the direction of the energy flow is reversed in some of the strokes. The device then works in a different operation mode [121, 124]. If, for example, the system absorbs heat from the cold reservoir in the third stroke, it functions as a refrigerator. The condition for refrigeration is

$$\frac{\omega_c}{\omega_h} < \frac{T_c}{T_h}. \tag{4.20}$$

4.3 Power and Efficiency

The two main performance indicators of a cyclic heat engine are its average power output

$$P = W/\bar{T}, \tag{4.21}$$

where W is the work in one cycle and $\bar{T}$ the cycle time, and its thermodynamic efficiency, which is defined as

$$\eta = W/Q_{\text{in}}. \tag{4.22}$$

Recall that $Q_{\text{in}} = Q^h$ is the heat input during one cycle. Due to the thermodynamic laws (4.17), the efficiency is universally bounded by the Carnot efficiency [22],

$$\eta \leq \eta_C = 1 - \frac{T_c}{T_h}. \tag{4.23}$$

For example, we find $\eta = 1 - \frac{\omega_c}{\omega_h}$ for the Otto cycle, which is less than the Carnot value due to the working condition (4.19). The bound is asymptotically saturated in the quasi-static limit $T_c\omega_h = T_h\omega_c$, where the system state is constant throughout the cycle. The power output of the engine, which is proportional to $(\bar{n}_h - \bar{n}_c)$, vanishes in this limit.

This behavior of the Otto cycle is generic for heat engines [22]; finite power is normally unattainable at the Carnot efficiency. To investigate the connection between power and efficiency in more detail, we plotted the power and the efficiency of the Otto engine as a function of the ratio ω_c/ω_h, see Fig. 4.2(a). The plot shows that the power output vanishes linearly both in the quasi-static limit and in the limit of zero driving amplitude. The maximum power is thus obtained at an intermediate efficiency. In Fig. 4.2(b), we compare the performance of the Otto engine at different values of the tunneling energy $\hbar\Delta$ and find that both efficiency and power decrease as Δ increases. This result indicates that

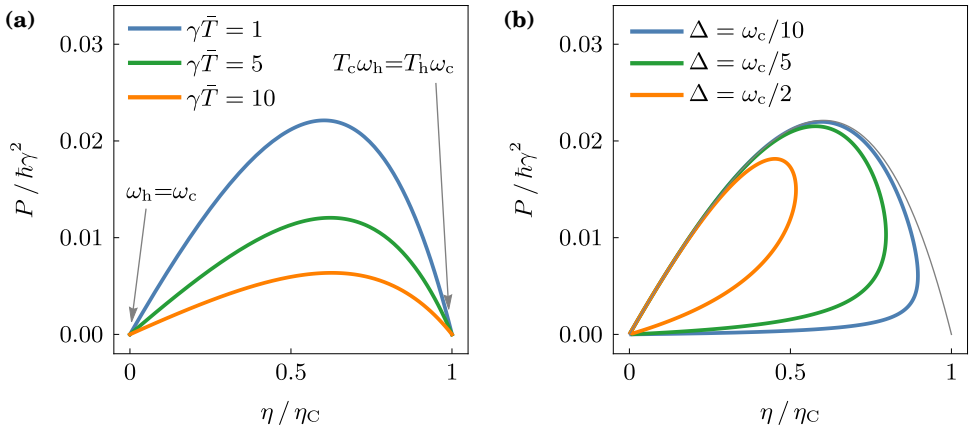

Figure 4.2. Power and efficiency of the Otto engine. The plots were obtained by varying ω_h between the values ω_c and $\omega_c T_h/T_c$ and keeping all other parameters fixed. We used the same coupling constant $\gamma = \gamma_c = \gamma_h$ for both the hot and the cold stroke and we assumed that the isentropic strokes are performed instantaneously. We set $\omega_c = \gamma$, $k_B T_h = \hbar\omega_c$ and $k_B T_c = \hbar\omega_c/2$. (a) Power-efficiency curves for the semi-classical Otto engine with $\Delta = 0$. The three curves correspond to different cycle times $\bar{T}$, where $t_c = t_h = \bar{T}/2$. (b) Power-efficiency curves for the quantum Otto engine with $t_c = t_h = 1/(2\gamma)$ and varying Δ. The thin gray line corresponds to $\Delta = 0$, i.e., to the top blue curve in panel (a).

the coherence that is created in the working substance at $\Delta > 0$ has a negative impact.

We note that there is no canonical choice of a classical counterpart to a quantum thermodynamic cycle. In Fig. 4.2(b), we assumed that the classical limit corresponds to taking the tunneling energy to zero while keeping the level splitting $\omega_{c,h}$ invariant. Alternatively, we might for example choose to keep the energy bias $\hbar\sqrt{\omega_{c,h}^2 - \Delta^2}$ invariant as Δ goes to zero; however, both choices qualitatively lead to the same results. To explain this behavior, we will in the remainder of this section discuss trade-off relations between power and efficiency, which govern the shape of the curves in Fig. 4.2. In particular, we will present the main result of Publication IV, a new trade-off relation for cyclic quantum heat engines operating far from equilibrium.

The trade-off relations that we study here have the general form

$$P \leq f[\eta] \tag{4.24}$$

with a function f satisfying $f[\eta_C] = 0$. In order to match the physical dimensions of power, f must depend on additional system characteristics. Relations of this type have recently been investigated for cyclic heat engines both in the classical regime [69, 117, 125, 126] and in the quantum regime close to equilibrium [33, 60]. An instructive example is the relation that was put forward in 2018 by Pietzonka and Seifert [127]. This relation is based on the thermodynamic uncertainty relation [128, 129]

$$\dot{S}^{\mathrm{tot}} \geq 2k_B \dot{X}^2 / D_X, \tag{4.25}$$

which holds for any net counting variable $X[\mathbb{T}]$ in a time-homogeneous classical Markov process [130–132]. Here, a net counting variable is a counting variable

with increments satisfying $x_t^{\mu\dagger} = -x_t^\mu$. Further, $\dot{S}^{\mathrm{tot}}$ and $\dot{X} = \partial_t \langle X \rangle_t$ are evaluated in the steady state and $D_X = \lim_{t\to\infty} t^{-1} \langle\langle X^2 \rangle\rangle_t$ is the rescaled variance of X. Applying the thermodynamic uncertainty relation to the net energy transfer from the reservoir to the system, i.e., to the heat Q, we obtain the relation [127]

$$P \leq \frac{1}{2} \frac{\eta_{\mathrm{C}} - \eta}{\eta} \frac{D_Q}{k_{\mathrm{B}} T_{\mathrm{c}}}, \tag{4.26}$$

which shows that in steady-state heat engines, the relationship between power and efficiency is controlled by the heat fluctuations.

In Publication IV, we derive a power-efficiency trade-off relation for reciprocating engines in two steps. First, we derive the bound

$$\Delta S^{m,\mathrm{j}} \geq 2 k_{\mathrm{B}} A_m \, \lambda_X^m \operatorname{artanh} \lambda_X^m \tag{4.27}$$

on the jump entropy production (4.11), which holds for any net counting variable $X[\mathbb{T}]$. This inequality plays a similar role here to the thermodynamic uncertainty relation (4.25) in that it bounds the entropy production beyond the second law. In Eq. (4.27), $\Delta S^{m,\mathrm{j}} = \int_0^{\bar{T}} \dot{S}_t^{m,\mathrm{j}} \, \mathrm{d}t$ is the jump entropy production in one driving period and

$$A_m = \sum_\mu^{(m)} \int_0^{\bar{T}} j_t^\mu \, \mathrm{d}t \tag{4.28}$$

is the activity of the m-th reservoir, in other words, the mean number of jump events associated with that reservoir in one cycle. The homogeneity λ_X^m is a statistical property of the single-jump distribution of the counting variable X. This distribution describes the relative frequency of events where the counting variable is incremented by x, it is given by

$$P_m[x] = \frac{1}{A_m} \sum_\mu^{(m)} \int_0^{\bar{T}} j_t^\mu \delta[x - x_t^\mu] \, \mathrm{d}t. \tag{4.29}$$

Homogeneity is a measure for the spread of this probability distribution,

$$\lambda_X^m = \sqrt{\mathbb{E}_m[x]^2 \,/\, \mathbb{E}_m[x^2]}, \tag{4.30}$$

which takes values between 0 and 1. Here, $\mathbb{E}_m$ denotes the expectation value with respect to the distribution $P_m[x]$.

The second step of our derivation consists of applying the bound (4.27) to the heat Q, obtaining

$$P \leq \eta \frac{A_{\mathrm{h}}}{\bar{T}} \sqrt{\mathbb{E}_{\mathrm{h}}[q^2]} \tanh\left[\frac{\Psi(\eta_{\mathrm{C}} - \eta)}{2 k_{\mathrm{B}} T_{\mathrm{c}}} \sqrt{\mathbb{E}_{\mathrm{h}}[q^2]} \right], \tag{4.31}$$

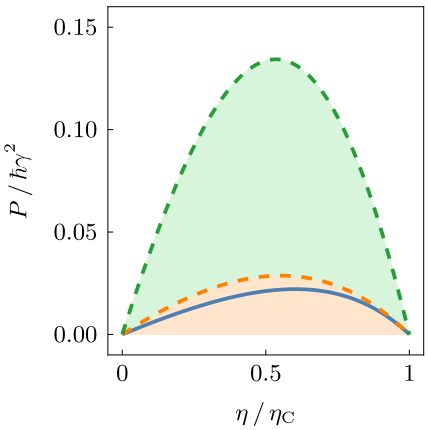

Figure 4.3. Power-efficiency trade-off relations applied to the qubit engine. The bottom blue curve is the actual power output of the Otto cycle. The center orange curve shows the bound (4.31) and the top green curve shows the weaker, protocol-independent bound (4.35). The parameters in this figure are the same as in Fig. 4.2(a) with $\gamma\bar{T} = 1$, i.e., the blue curves in both plots are identical.

where the ratio

$$\Psi = \frac{\Delta S^{\mathrm{j}}}{\Delta S^{\mathrm{tot}}} = \sum\nolimits_m \frac{\Delta S^{m,\mathrm{j}}}{\Delta S^{\mathrm{tot}}} \leq 1 \tag{4.32}$$

quantifies the effect of coherence. Equation (4.31) shows that, for cyclic heat engines, the relationship between power and efficiency is governed by the second single-jump moment of the heat uptake. Similar results apply to other types of thermal machines. Further, the bounds become weaker as coherence decreases, and they are weakest in the semi-classical limit with $\Psi = 1$. Coherence can therefore be seen as detrimental for the performance of thermal machines in the adiabatic weak-coupling regime.

Our result constitutes a generalization of the trade-off relations derived by Brandner *et al.* in Refs. [33, 60] for quantum heat engines in linear response [PIV]. Using $\tanh x \leq x$ and $\psi \leq 1$, we also recover the relation

$$P \leq \eta(\eta_{\mathrm{C}} - \eta)\frac{\Theta}{k_{\mathrm{B}} T_{\mathrm{c}}} \quad \text{with} \quad \Theta = \frac{1}{2\bar{T}} \sum\nolimits_{\mu}^{(\mathrm{h})} \int_0^{\bar{T}} j_t^{\mu} (\varepsilon_t^{\mu})^2 \, \mathrm{d}t, \tag{4.33}$$

which was derived by Shiraishi and coworkers for classical devices [125, 126].

By applying additional approximations, the inequality (4.31) can be transformed into a protocol-independent relation between power and efficiency. For example, for a qubit engine, we can bound the term $\sqrt{\mathbb{E}_h[q^2]}$ by $\hbar\bar{\omega}$, the maximum admissible level splitting, and we can bound the activity of the hot reservoir by

$$\bar{A}_{\mathrm{h}} = \frac{\gamma t_{\mathrm{h}}}{1 - \mathrm{e}^{-\hbar\bar{\omega}\beta_{\mathrm{h}}}}. \tag{4.34}$$

In this way, we obtain the relation

$$P \leq \eta \frac{\hbar\bar{\omega}}{\bar{T}} \bar{A}_{\mathrm{h}} \tanh \frac{\hbar\bar{\omega}(\eta_{\mathrm{C}} - \eta)}{2k_{\mathrm{B}} T_{\mathrm{c}}}, \tag{4.35}$$

which holds for all cyclic single-qubit heat engines. However, as shown in Fig. 4.3, it can be significantly weaker than the bound (4.31).

4.4 Quantum Amplifiers

Thermodynamic cycles that consist of only thermalization and classical driving are semi-classical, they do not generate coherence. In this section, we follow Publication V and study the opposite limit, that is, cycles that consist of only thermalization and coherent driving [63]. Hence, we require the system Hamiltonian to have the general form

$$H_t = V_t \bar{H} V_t^{\dagger}, \tag{4.36}$$

where $\bar{H}$ is a time-independent Hermitian operator and V_t are unitary transformations. Quantum heat engines with Hamiltonians of this form are called quantum amplifiers [73, 133].

The study of quantum amplifiers was initiated in 1959, when Scovil and Schulz-DuBois recognized that the three-level maser can be understood as a

heat engine [72]. The power generation mechanism of this device is based purely on quantum effects: due to stimulated emission, the maser emits photons into the coherent light mode of a surrounding cavity. The resulting amplification of the light mode plays the role of the work output of the heat engine. Over the years, these ideas have inspired a multitude of studies on the nature of power generation in quantum systems, see for instance Refs. [21, 133–139], and it has recently become possible to realize this type of setup also in the lab [15, 140].

In Sec. 2.4, we introduced the cyclic 3-level maser and investigated the dynamics of its limit cycle. We now continue our analysis of this device by studying its thermodynamic performance. As we recall, the control protocol consists of the three strokes depicted in Fig. 2.3. In the first stroke, the maser absorbs the energy

$$Q_{\mathrm{in}} = U_{(1)} - U_{(0)} = \frac{(\mathrm{e}^{\beta_{\mathrm{c}}\varepsilon_{21}} - \mathrm{e}^{\beta_{\mathrm{h}}\varepsilon_{31}})}{(2+\mathrm{e}^{\beta_{\mathrm{c}}\varepsilon_{21}})(1+\mathrm{e}^{\beta_{\mathrm{h}}\varepsilon_{31}})}\,\varepsilon_{31} \tag{4.37}$$

from the hot reservoir, where β_{c} and β_{h} are the inverse temperatures of the reservoirs and ε_{nm} the level separations. The subscript (k) indicates that the energy is evaluated at the end of the k-th stroke. The energy extracted from the system in the second stroke corresponds to the work output

$$W = U_{(1)} - U_{(2)} = \varepsilon_{32}(p^3_{(1)} - p^2_{(1)}) = \frac{(\mathrm{e}^{\beta_{\mathrm{c}}\varepsilon_{21}} - \mathrm{e}^{\beta_{\mathrm{h}}\varepsilon_{31}})}{(2+\mathrm{e}^{\beta_{\mathrm{c}}\varepsilon_{21}})(1+\mathrm{e}^{\beta_{\mathrm{h}}\varepsilon_{31}})}\,\varepsilon_{32}. \tag{4.38}$$

In the third stroke, the remaining energy $Q_{\mathrm{out}} = Q_{\mathrm{in}} - W$ is deposited into the cold reservoir as waste heat. Note that Eqs. (4.37) and (4.38) are valid in the limit of long thermalization times. To function as a heat engine, the device must satisfy the working condition [72]

$$\frac{\varepsilon_{21}}{\varepsilon_{31}} \geq \frac{T_{\mathrm{c}}}{T_{\mathrm{h}}}. \tag{4.39}$$

Its thermodynamic efficiency is then [72]

$$\eta = \frac{W}{Q_{\mathrm{in}}} = 1 - \frac{\varepsilon_{21}}{\varepsilon_{31}} \leq \eta_{\mathrm{C}}. \tag{4.40}$$

The operation principle of any quantum amplifier relies on the possibility to create population inversion in the system, which can then be converted into useful work as illustrated in Eq. (4.38). In the 3-level maser, population inversion is created using energy filters, which make it possible to couple each reservoir to only a single transition. In Publication V, we ask whether other mechanisms of creating population inversion are possible, and which conditions a working medium must generally satisfy to be able to amplify light in cyclic operation. To answer these questions, we study the flow of ergotropy in the system. Ergotropy is the maximum amount of work that can be obtained from a system by applying unitary operations [141–143],

$$\mathscr{E}_t = \mathrm{tr}\left[H_t \rho_t\right] - \min_R \mathrm{tr}\left[H_t R \rho_t R^\dagger\right], \tag{4.41}$$

and can be regarded as a measure of population inversion. Here, the minimum is taken over all unitary transformations R. In quantum amplifiers, the ergotropy satisfies the flow equation

$$\dot{\mathscr{E}}_t = -\dot{W}_t + \mathscr{J}_t, \quad \text{where} \quad \mathscr{J}_t = \sum\nolimits_n E^n \left(\langle n_t | \hat{L}_t \rho_t | n_t \rangle - \langle r_t^n | \hat{L}_t \rho_t | r_t^n \rangle \right) \tag{4.42}$$

is the reservoir-induced ergotropy production. The eigenvalues r_t^n of ρ_t and E^n of H_t are ordered so that $r_t^n \leq r_t^m$ for $E^n \geq E^m$, and $|r_t^n\rangle$ and $|n_t\rangle$ are the corresponding eigenstates. Integrating Eq. (4.42) over one period shows that $W = \int_0^{\bar{T}} \mathscr{J}_t \, \mathrm{d}t$. This result formally confirms that a cyclic quantum amplifier can only function as a heat engine with positive work output if the reservoirs are able to create ergotropy in the working system, i.e., only if the quantity $\mathscr{J}_t$ can become positive at all in the setup.

The main result of Publication V is a working condition for cyclic quantum amplifiers, which identifies a large class of systems where $\mathscr{J}_t$ is always negative. This class of systems consists of ladder systems, that is, quantum systems with equally spaced energy levels and a Hamiltonian of the form $H_t = \hbar\omega \sum_n n |n_t\rangle\langle n_t|$. The dimension of the system Hilbert space may be finite or infinite. The state follows the Lindblad equation

$$\begin{aligned} \dot{\rho}_t = \frac{1}{\mathrm{i}\hbar}[H_t, \rho_t] &+ \gamma(\bar{n}+1)\left(V_t^{\downarrow} \rho_t V_t^{\uparrow} - \frac{1}{2}\left\{ V_t^{\uparrow} V_t^{\downarrow}, \rho_t \right\} \right) \\ &+ \gamma\bar{n}\left(V_t^{\uparrow} \rho_t V_t^{\downarrow} - \frac{1}{2}\left\{ V_t^{\downarrow} V_t^{\uparrow}, \rho_t \right\} \right), \end{aligned} \tag{4.43}$$

which contains both Eq. (2.19) and Eq. (3.20) as special cases. The creation and annihilation operators are

$$V_t^{\uparrow} = \sum\nolimits_n n^{\alpha} \, |(n+1)_t\rangle\langle n_t| \quad \text{and} \quad V_t^{\downarrow} = (V_t^{\uparrow})^{\dagger}, \tag{4.44}$$

where the exponent α determines the scaling of the weighting factors. The class of systems that are identified as unsuitable by our working condition consists of all ladder systems with $0 \leq \alpha \leq 1/2$. In particular, both the damped qubit and the damped quantum harmonic oscillator are not suitable working media for quantum amplifiers.

Our result raises the question whether it is possible to create a cyclic quantum amplifier using a ladder system with, e.g., $\alpha > 1/2$. In Publication V, we answer this question affirmatively and propose a new type of cyclic quantum amplifier based on ladder systems, see Fig. 4.4. Here, the necessary population inversion arises during the incomplete relaxation of a metastable state. Since the environment couples to all energy levels of the quantum ladder, our proposed setup does not rely on the use of energy filters like the conventional 3-level maser.

Overall, our results indicate that quantum amplification is surprisingly difficult and requires a minimum amount of structure in either the system or the system-bath coupling. This statement can be further corroborated by considering the ergotropy flow of systems close to equilibrium. We hence assume that the state of the system has the form

$$\rho_t = \rho_t^{\mathrm{eq}}[\beta_t] + \varepsilon\sigma_t, \tag{4.45}$$

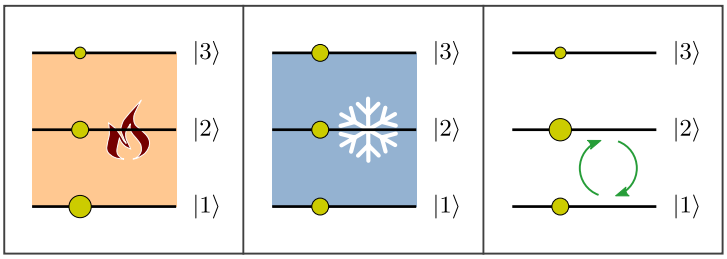

Figure 4.4. Control protocol of a cyclic quantum amplifier based on a 3-level quantum ladder. The three panels correspond to the three strokes, which are applied periodically. In the first stroke, the system thermalizes at a high temperature for a long time. The populations, symbolized by the yellow circles, are therefore approximately equally distributed at the beginning of the second stroke, where the system thermalizes at a low temperature. Due to the form (4.44) of the Lindblad operators with $\alpha > 1/2$, the thermalization creates population inversion between levels $|1\rangle$ and $|2\rangle$ on an intermediate time scale. The thermalization is interrupted at the point of maximum population inversion, which is is used in the third stroke to extract work.

where ε is small and σ_t is a traceless operator. Inserting (4.45) into the definition of the reservoir-induced ergotropy production shows that

$$\mathscr{J}_t = -\mathscr{J}_t^{(2)}\varepsilon^2 + \mathscr{O}(\varepsilon^3), \tag{4.46}$$

where $\mathscr{J}_t^{(2)}$ is a positive expression. This result is valid for any system dynamics in the form of a Lindblad master equation satisfying detailed balance. Cyclic quantum amplification is therefore impossible close to equilibrium, as shown previously in Refs. [37, 60].

4.5 Optimal Control of Thermal Machines

We conclude our analysis of cyclic thermal machines by analyzing the thermodynamic performance of a concrete setup, a single qubit refrigerator. The main performance indicators of a cyclic refrigerator are the cooling power

$$P^{\mathrm{c}} = Q^{\mathrm{c}}/\bar{T} \tag{4.47}$$

and the coefficient of performance

$$\eta = -Q^{\mathrm{c}}/W \quad \text{with} \quad \eta \leq \eta_{\mathrm{C}} = \frac{T_{\mathrm{c}}}{T_{\mathrm{h}} - T_{\mathrm{c}}}, \tag{4.48}$$

where Q^{c} is the heat extracted from the cold reservoir and $(-W)$ the work input in one period. The Carnot bound (4.48) follows from the second law. Our aim in Publication VI is to determine the optimal control protocols that maximize either the cooling power or, for fixed cooling power, the coefficient of performance.

The setup consists of a superconducting qubit which is coupled to two resonant circuits acting as thermal reservoirs, see Fig. 4.5(a). The Lindblad equation describing the system dynamics has the form

$$\dot{\rho}_t = \frac{1}{\mathrm{i}\hbar}[H_t, \rho_t] + \hat{D}_t^{\mathrm{h}}\rho_t + \hat{D}_t^{\mathrm{c}}\rho_t, \tag{4.49}$$

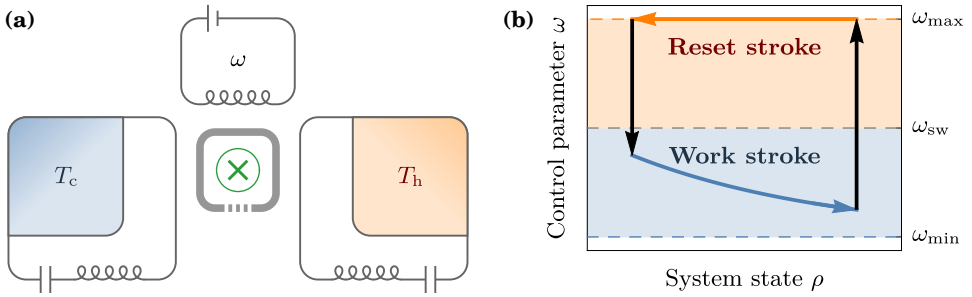

Figure 4.5. Quantum refrigerator based on a superconducting qubit. (a) Sketch of the experimental setup described in Refs. [122, 123, 144]. The central superconducting qubit is coupled to two resonant circuits, which play the role of thermal reservoirs with temperatures T_c and $T_h > T_c$. The current in an additional bias circuit controls the magnetic flux in the qubit, and thus its level splitting $\hbar\omega$. (b) Depending on the level splitting, the qubit is either coupled to the cold ($\omega_{min} \le \omega \le \omega_{sw}$) or the hot ($\omega_{sw} \le \omega \le \omega_{max}$) reservoir. One operation cycle of the refrigerator consists of a work stroke (blue arrow), where the system extracts heat from the cold reservoir, and a reset stroke (orange arrow), where the system state is reset to its initial value. In between, the value of the control parameter ω is changed instantaneously (black arrows). Both figures adapted from Publication VI.

where the qubit Hamiltonian H_t was given in Eq. (4.14) and the dissipators are

$$\begin{aligned}\hat{D}_t^m \rho_t = \Gamma_m[\omega_t]\left(\sigma_t^\downarrow \rho_t \sigma_t^\uparrow - \frac{1}{2}\left\{\sigma_t^\uparrow \sigma_t^\downarrow, \rho_t\right\}\right) + \\ \Gamma_m[\omega_t] e^{-\hbar\omega_t/(k_B T_m)}\left(\sigma_t^\uparrow \rho_t \sigma_t^\downarrow - \frac{1}{2}\left\{\sigma_t^\downarrow \sigma_t^\uparrow, \rho_t\right\}\right)\end{aligned} \tag{4.50}$$

for $m = c, h$. The coupling $\Gamma_m[\omega]$ of the system to the m-th reservoir is strong if the frequency ω is close to the resonance frequency of the resonant circuit, and weak otherwise. We assume that the dependence of the couplings on the level splitting has the form

$$\Gamma_c[\omega] = \begin{cases} \gamma & \omega_{min} \le \omega \le \omega_{sw} \\ 0 & \text{otherwise} \end{cases} \quad \text{and} \quad \Gamma_h[\omega] = \begin{cases} \gamma & \omega_{sw} \le \omega \le \omega_{max} \\ 0 & \text{otherwise} \end{cases}. \tag{4.51}$$

Therefore, Γ_c is only non-zero if ω is below the switching value ω_{sw}, and Γ_h is only non-zero if ω is above ω_{sw}, see Fig. 4.5(b). This simple dependence of Γ_m on ω enables us to carry out the optimization of the the semi-classical refrigerator analytically. We expect that numerical calculations based on more realistic models, such as the one introduced in Ref. [122], would not lead to qualitatively different results.

Since the reservoir couplings are functions of the level splitting $\hbar\omega$ and cannot be changed independently, the refrigerator is operated with only a single control parameter. The quantities P^c and η can be understood as functionals of the control protocol ω_t and can therefore be maximized using the calculus of variations and other standard techniques of optimal control theory [145]. These methods have been used, for example, in Refs. [146–153] to study the optimal performance of nanoscopic devices. The direct application of optimal control theory to our model system is however difficult in practice, since the Euler-Lagrange equations have to be solved with periodic boundary conditions under the differential constraint posed by the Lindblad equation.

To simplify the optimization problem, we observe that each control cycle can be split into two strokes, because the qubit can only couple to one reservoir at a time. The two strokes are the work stroke, in which the qubit extracts heat from the cold reservoir, and the reset stroke, where the interaction with the hot circuit brings the state of the qubit back to its initial value, see Fig. 4.5(b). We can thus perform the optimization in two steps, following the two-stroke optimization scheme introduced in Publication VI. In the first step, we fix an arbitrary switching time t_{sw} and arbitrary boundary conditions ρ_0 and $\rho_{t_{\mathrm{sw}}}$. We then optimize both the work stroke at times $0 \leq t \leq t_{\mathrm{sw}}$ and the reset stroke at times $t_{\mathrm{sw}} \leq t \leq \bar{T}$ with the given boundary conditions, see Fig. 4.6. These optimizations can be carried out analytically. In the second step, we numerically maximize over the remaining parameters t_{sw}, ρ_0 and $\rho_{t_{\mathrm{sw}}}$.

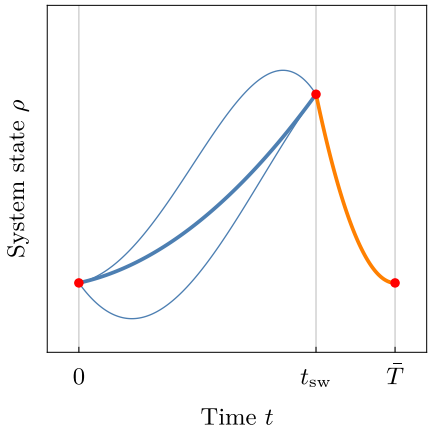

Figure 4.6. Illustration of our two-stroke optimization scheme, adapted from Publication VI. The figure shows the trajectory of the system state in the work stroke (blue) and in the reset stroke (orange). The thin lines correspond to small displacements of the work stroke protocol, which keep the red points of the trajectory fixed.

As the example in Fig. 4.7(a) demonstrates, the optimal protocols can be rather complex. The plot shows the control protocol that maximizes the coefficient of performance for a fixed cooling power in the semi-classical regime. Its reset stroke consists of three segments, with the protocol being constant in the first and in the third segment. This form of the protocol is a manifestation of Pontryagin's minimum principle, which states that, if a control parameter is restricted to a finite interval, the optimal protocol might run along the boundaries of the interval [145, 153–155]. On the non-constant segments, the optimal control protocol has the general form [PVI]

$$\hbar\omega_t = k_{\mathrm{B}} T_m \log\left[\frac{2 - 2c_1 W_m[c_2 \mathrm{e}^{-\gamma t}]}{c_1 W_m[c_2 \mathrm{e}^{-\gamma t}]^2} - 1\right], \tag{4.52}$$

where c_1 and c_2 are integration constants and W_{c} (W_{h}) is the negative (positive) branch of the Lambert W function.

Figure 4.7(b) shows a plot of the maximum cooling power of the single qubit refrigerator as a function of its tunneling energy $\hbar\Delta$. In accordance with our other results, we find that the performance of the refrigerator decreases as the coherence is increased. At large values of Δ, the maximum cooling power reaches zero, i.e., the device is not able to function any more. We note that the results for finite Δ were obtained in the adiabatic regime. Repeating the analysis in the fast-driving regime qualitatively yields the same results [PVI]; we thus expect our results to apply also at intermediate frequencies.

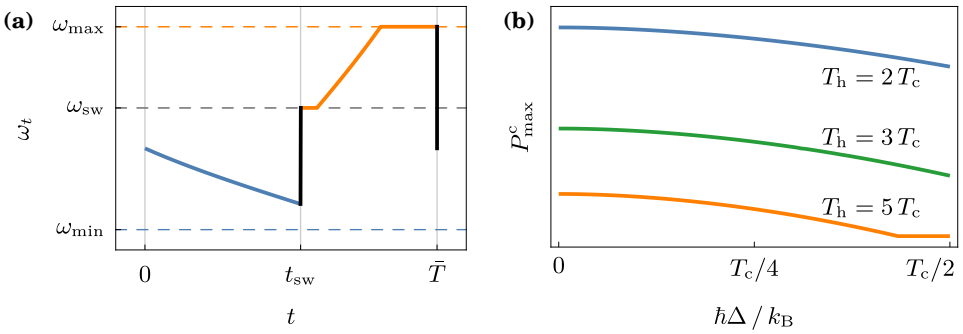

Figure 4.7. Selected results of the refrigerator optimization. (a) Control protocol that maximizes the coefficient of performance at the fixed cooling power $P^{\mathrm{c}} = 0.9P^{\mathrm{c}}_{\max}$, where $P^{\mathrm{c}}_{\max}$ is the maximum cooling power. Here, the tunneling energy Δ was set to 0. (b) Maximum cooling power in the adiabatic regime as a function of the tunneling energy $\hbar\Delta$ for different temperatures of the hot reservoir. The figures correspond to Figs. 6(b) and 8(a) of Publication VI, which we refer to for detailed listings of the used system parameters.

5. Conclusions

In this dissertation, we set out to study the effects of coherence on cyclic thermal machines operating in the adiabatic weak-coupling regime. The first part of the thesis focused on fundamental problems: we investigated the relaxation process of periodically driven open quantum systems [PI] as well as basic properties of thermodynamic currents in quantum-scale setups [PII, PIII]. The second part of the thesis was devoted to the analysis of the performance of thermal machines. We were able to derive a universal trade-off relation between the two main performance indicators, power and efficiency, which is valid in the quantum regime and far from equilibrium [PIV]. Our bound indicates that the Pareto frontier of power and efficiency recedes monotonically when the coherence increases. This performance decrease can also be seen in the concrete example of a single-qubit thermal machine, where the amount of coherence can be controlled with a single parameter Δ. Our analysis of this device shows that its performance decreases with increasing coherence, even if the control protocol is optimized for each value of Δ separately [PVI]. In addition, we studied cyclic quantum amplifiers, machines with a power generation mechanism that is based purely on quantum effects, and found that they are subject to much stronger working conditions than conventional heat engines. They can neither function close to equilibrium nor with "too simple" working systems such as qubits or harmonic oscillators [PV].

Our findings can be interpreted as the result of a trade-off between two opposing effects as we move from the classical to the quantum regime. On the one hand, the number of accessible degrees of freedom increases and thus our control over the system improves and new mechanisms for power generation arise. On the other hand, as we saw in Sec. 4.1, increased coherence is associated with higher irreversible entropy production, a phenomenon known as quantum friction [32, 156, 157]. Overall, our results show that quantum friction generally outweighs the potential advantages of quantum effects in the adiabatic weak-coupling regime. The amount of coherence in the working substance of a thermal machine should thus be minimized in order to achieve optimal performance.

The situation might be different in other operation regimes. Recent results have, for example, shown advantages of quantum effects in the regimes of strong

coupling and fast driving [158–161]. Systematic investigations of the thermodynamics of strongly coupled systems are however complicated by the fact that some fundamental questions have not yet been conclusively answered. For example, it is unclear how heat and work should be identified if the interaction energy between system and reservoir is non-negligible, see for instance Ref. [162]. It remains a challenge for future investigations to formulate a consistent framework of thermodynamics in such scenarios, and to clearly point out quantum advantages in strongly coupled systems.

References

[1] H.-P. Breuer and F. Petruccione, *The Theory of Open Quantum Systems* (Oxford University Press, Oxford, 2002).

[2] J. P. Dowling and G. J. Milburn, *Quantum technology: The second quantum revolution*, Philos. Trans. Royal Soc. A **361**, 1655 (2003).

[3] T. D. Ladd, F. Jelezko, R. Laflamme, Y. Nakamura, C. Monroe, and J. L. O'Brien, *Quantum computers*, Nature **464**, 45 (2010).

[4] W. H. Zurek, *Decoherence and the Transition from Quantum to Classical*, Phys. Today **44**, 36 (1991).

[5] F. Giazotto, T. T. Heikkilä, A. Luukanen, A. M. Savin, and J. P. Pekola, *Opportunities for mesoscopics in thermometry and refrigeration: Physics and applications*, Rev. Mod. Phys. **78**, 217 (2006).

[6] V. Gorini, A. Frigerio, M. Verri, A. Kossakowski, and E. C. G. Sudarshan, *Properties of quantum Markovian master equations*, Rep. Math. Phys. **13**, 149 (1978).

[7] S. Vinjanampathy and J. Anders, *Quantum thermodynamics*, Contemp. Phys. **57**, 545 (2016).

[8] J. Millen and A. Xuereb, *Perspective on quantum thermodynamics*, New J. Phys. **18**, 011002 (2016).

[9] F. Binder, L. A. Correa, C. Gogolin, J. Anders, and G. Adesso, eds., *Thermodynamics in the Quantum Regime: Fundamental Aspects and New Directions*, Fundamental Theories of Physics, Vol. 195 (Springer International Publishing, Cham, 2018).

[10] D. Gelbwaser-Klimovsky and A. Aspuru-Guzik, *Strongly Coupled Quantum Heat Machines*, J. Phys. Chem. Lett. **6**, 3477 (2015).

[11] U. Seifert, *First and Second Law of Thermodynamics at Strong Coupling*, Phys. Rev. Lett. **116**, 020601 (2016).

[12] M. W. Zemansky and R. H. Dittman, *Heat and Thermodynamics: An Intermediate Textbook* (McGraw-Hill, 1997).

[13] J. P. Pekola, *Towards quantum thermodynamics in electronic circuits*, Nature Phys **11**, 118 (2015).

[14] J. Roßnagel, S. T. Dawkins, K. N. Tolazzi, O. Abah, E. Lutz, F. Schmidt-Kaler, and K. Singer, *A single-atom heat engine*, Science **352**, 325 (2016).

[15] J. Klatzow, J. N. Becker, P. M. Ledingham, C. Weinzetl, K. T. Kaczmarek, D. J. Saunders, J. Nunn, I. A. Walmsley, R. Uzdin, and E. Poem, *Experimental Demonstration of Quantum Effects in the Operation of Microscopic Heat Engines*, Phys. Rev. Lett. **122**, 110601 (2019).

[16] J. T. Muhonen, M. Meschke, and J. P. Pekola, *Micrometre-scale refrigerators*, Rep. Prog. Phys. **75**, 046501 (2012).

[17] M. O. Scully, M. S. Zubairy, G. S. Agarwal, and H. Walther, *Extracting work from a single heat bath via vanishing quantum coherence*, Science **299**, 862 (2003).

[18] O. Abah and E. Lutz, *Efficiency of heat engines coupled to nonequilibrium reservoirs*, EPL **106**, 20001 (2014).

[19] J. Roßnagel, O. Abah, F. Schmidt-Kaler, K. Singer, and E. Lutz, *Nanoscale Heat Engine Beyond the Carnot Limit*, Phys. Rev. Lett. **112**, 030602 (2014).

[20] R. Alicki, *The quantum open system as a model of the heat engine*, J. Phys. A **12**, L103 (1979).

[21] R. Uzdin, A. Levy, and R. Kosloff, *Equivalence of Quantum Heat Machines, and Quantum-Thermodynamic Signatures*, Phys. Rev. X **5**, 031044 (2015).

[22] D. Gelbwaser-Klimovsky, W. Niedenzu, and G. Kurizki, *Chapter Twelve - Thermodynamics of Quantum Systems Under Dynamical Control*, in *Advances In Atomic, Molecular, and Optical Physics*, Vol. 64, edited by E. Arimondo, C. C. Lin, and S. F. Yelin (Academic Press, 2015) pp. 329–407.

[23] K. Maruyama, F. Nori, and V. Vedral, *Colloquium: The physics of Maxwell's demon and information*, Rev. Mod. Phys. **81**, 1 (2009).

[24] K. Funo, M. Ueda, and T. Sagawa, *Quantum Fluctuation Theorems*, in *Thermodynamics in the Quantum Regime*, Fundamental Theories of Physics, Vol. 195, edited by F. Binder, L. A. Correa, C. Gogolin, J. Anders, and G. Adesso (Springer International Publishing, Cham, 2018) pp. 249–273.

[25] M. O. Scully, K. R. Chapin, K. E. Dorfman, M. B. Kim, and A. Svidzinsky, *Quantum heat engine power can be increased by noise-induced coherence*, PNAS **108**, 15097 (2011).

[26] U. Harbola, S. Rahav, and S. Mukamel, *Quantum heat engines: A thermodynamic analysis of power and efficiency*, EPL **99**, 50005 (2012).

[27] K. Funo, Y. Watanabe, and M. Ueda, *Thermodynamic work gain from entanglement*, Phys. Rev. A **88**, 052319 (2013).

[28] N. Brunner, M. Huber, N. Linden, S. Popescu, R. Silva, and P. Skrzypczyk, *Entanglement enhances cooling in microscopic quantum refrigerators*, Phys. Rev. E **89**, 032115 (2014).

[29] K. Brandner, M. Bauer, M. T. Schmid, and U. Seifert, *Coherence-enhanced efficiency of feedback-driven quantum engines*, New J. Phys. **17**, 065006 (2015).

[30] R. Uzdin, *Coherence-Induced Reversibility and Collective Operation of Quantum Heat Machines via Coherence Recycling*, Phys. Rev. Appl. **6**, 024004 (2016).

[31] G. Watanabe, B. P. Venkatesh, P. Talkner, and A. del Campo, *Quantum Performance of Thermal Machines over Many Cycles*, Phys. Rev. Lett. **118**, 050601 (2017).

[32] R. Kosloff, *Quantum Thermodynamics: A Dynamical Viewpoint*, Entropy **15**, 2100 (2013).

[33] K. Brandner, M. Bauer, and U. Seifert, *Universal Coherence-Induced Power Losses of Quantum Heat Engines in Linear Response*, Phys. Rev. Lett. **119**, 170602 (2017).

[34] W. Niedenzu, V. Mukherjee, A. Ghosh, A. G. Kofman, and G. Kurizki, *Quantum engine efficiency bound beyond the second law of thermodynamics*, Nat Commun **9**, 165 (2018).

[35] J. P. Pekola, B. Karimi, G. Thomas, and D. V. Averin, *Supremacy of incoherent sudden cycles*, Phys. Rev. B **100**, 085405 (2019).

[36] J. P. Santos, L. C. Céleri, G. T. Landi, and M. Paternostro, *The role of quantum coherence in non-equilibrium entropy production*, npj Quantum Inf **5**, 1 (2019).

[37] K. Brandner and K. Saito, *Thermodynamic Geometry of Microscopic Heat Engines*, Phys. Rev. Lett. **124**, 040602 (2020).

[38] T. Qiu, Z. Fei, R. Pan, and H. T. Quan, *Quantum corrections to the entropy and its application in the study of quantum Carnot engines*, Phys. Rev. E **101**, 032113 (2020).

[39] A. Friedenberger and E. Lutz, *When is a quantum heat engine quantum?*, EPL **120**, 10002 (2017).

[40] S. Nakajima, *On Quantum Theory of Transport Phenomena: Steady Diffusion*, Prog. Theor. Phys. **20**, 948 (1958).

[41] R. Zwanzig, *Ensemble Method in the Theory of Irreversibility*, J. Chem. Phys. **33**, 1338 (1960).

[42] A. O. Caldeira and A. J. Leggett, *Path integral approach to quantum Brownian motion*, Physica A **121**, 587 (1983).

[43] M. Esposito, M. A. Ochoa, and M. Galperin, *Quantum Thermodynamics: A Nonequilibrium Green's Function Approach*, Phys. Rev. Lett. **114**, 080602 (2015).

[44] J. Iles-Smith, N. Lambert, and A. Nazir, *Environmental dynamics, correlations, and the emergence of noncanonical equilibrium states in open quantum systems*, Phys. Rev. A **90**, 032114 (2014).

[45] P. Strasberg, G. Schaller, T. L. Schmidt, and M. Esposito, *Fermionic reaction coordinates and their application to an autonomous Maxwell demon in the strong-coupling regime*, Phys. Rev. B **97**, 205405 (2018).

[46] R. P. Feynman and F. L. Vernon, *The theory of a general quantum system interacting with a linear dissipative system*, Ann. Phys. (N. Y.) **24**, 118 (1963).

[47] J. T. Stockburger and C. H. Mak, *Stochastic Liouvillian algorithm to simulate dissipative quantum dynamics with arbitrary precision*, J. Chem. Phys. **110**, 4983 (1999).

[48] A. Kato and Y. Tanimura, *Hierarchical Equations of Motion Approach to Quantum Thermodynamics*, in *Thermodynamics in the Quantum Regime*, Fundamental Theories of Physics, edited by F. Binder, L. A. Correa, C. Gogolin, J. Anders, and G. Adesso (Springer International Publishing, Cham, 2018) pp. 579–595.

[49] D. Tamascelli, A. Smirne, S. F. Huelga, and M. B. Plenio, *Nonperturbative Treatment of non-Markovian Dynamics of Open Quantum Systems*, Phys. Rev. Lett. **120**, 030402 (2018).

[50] N. Lambert, S. Ahmed, M. Cirio, and F. Nori, *Modelling the ultra-strongly coupled spin-boson model with unphysical modes*, Nat Commun **10**, 1 (2019).

[51] D. Manzano, *A short introduction to the Lindblad master equation*, AIP Advances **10**, 025106 (2020).

[52] Á. Rivas and S. F. Huelga, *Open Quantum Systems. An Introduction*, SpringerBriefs in Physics (Springer, Berlin, Heidelberg, 2012).

[53] D. Chruściński and A. Kossakowski, *Markovianity criteria for quantum evolution*, J. Phys. B **45**, 154002 (2012).

[54] H.-P. Breuer, E.-M. Laine, J. Piilo, and B. Vacchini, *Non-Markovian dynamics in open quantum systems*, Rev. Mod. Phys. **88**, 021002 (2016).

[55] V. Gorini, A. Kossakowski, and E. C. G. Sudarshan, *Completely positive dynamical semigroups of N-level systems*, J. Math. Phys. **17**, 821 (1976).

[56] G. Lindblad, *On the generators of quantum dynamical semigroups*, Commun. Math. Phys. **48**, 119 (1976).

[57] D. A. Lidar, Z. Bihary, and K. B. Whaley, *From completely positive maps to the quantum Markovian semigroup master equation*, Chem. Phys. **268**, 35 (2001).

[58] C. Majenz, T. Albash, H.-P. Breuer, and D. A. Lidar, *Coarse graining can beat the rotating-wave approximation in quantum Markovian master equations*, Phys. Rev. A **88**, 012103 (2013).

[59] H.-P. Breuer and F. Petruccione, *Dissipative quantum systems in strong laser fields: Stochastic wave-function method and Floquet theory*, Phys. Rev. A **55**, 3101 (1997).

[60] K. Brandner and U. Seifert, *Periodic thermodynamics of open quantum systems*, Phys. Rev. E **93**, 062134 (2016).

[61] I. Chiorescu, Y. Nakamura, C. J. P. M. Harmans, and J. E. Mooij, *Coherent Quantum Dynamics of a Superconducting Flux Qubit*, Science **299**, 1869 (2003).

[62] J. P. S. Peterson, T. B. Batalhão, M. Herrera, A. M. Souza, R. S. Sarthour, I. S. Oliveira, and R. M. Serra, *Experimental Characterization of a Spin Quantum Heat Engine*, Phys. Rev. Lett. **123**, 240601 (2019).

[63] M. Scandi, H. J. D. Miller, J. Anders, and M. Perarnau-Llobet, *Quantum work statistics close to equilibrium*, arXiv:1911.04306 [quant-ph] (2019).

[64] H. Spohn, *An algebraic condition for the approach to equilibrium of an open N-level system*, Lett. Math. Phys **2**, 33 (1977).

[65] T. Feldmann and R. Kosloff, *Characteristics of the limit cycle of a reciprocating quantum heat engine*, Phys. Rev. E **70**, 046110 (2004).

[66] A. Ghosh, C. L. Latune, L. Davidovich, and G. Kurizki, *Catalysis of heat-to-work conversion in quantum machines*, PNAS **114**, 12156 (2017).

[67] R. Kosloff and Y. Rezek, *The Quantum Harmonic Otto Cycle*, Entropy **19**, 136 (2017).

[68] A. C. Barato, R. Chetrite, A. Faggionato, and D. Gabrielli, *Bounds on current fluctuations in periodically driven systems*, New J. Phys. **20**, 103023 (2018).

[69] T. Koyuk and U. Seifert, *Operationally Accessible Bounds on Fluctuations and Entropy Production in Periodically Driven Systems*, Phys. Rev. Lett. **122**, 230601 (2019).

[70] Z. Gong, R. Hamazaki, and M. Ueda, *Discrete Time-Crystalline Order in Cavity and Circuit QED Systems*, Phys. Rev. Lett. **120**, 040404 (2018).

[71] F. M. Gambetta, F. Carollo, M. Marcuzzi, J. P. Garrahan, and I. Lesanovsky, *Discrete Time Crystals in the Absence of Manifest Symmetries or Disorder in Open Quantum Systems*, Phys. Rev. Lett. **122**, 015701 (2019).

[72] H. E. D. Scovil and E. O. Schulz-DuBois, *Three-Level Masers as Heat Engines*, Phys. Rev. Lett. **2**, 262 (1959).

[73] E. Geva and R. Kosloff, *Three-level quantum amplifier as a heat engine: A study in finite-time thermodynamics*, Phys. Rev. E **49**, 3903 (1994).

[74] U. Seifert, *Stochastic thermodynamics: From principles to the cost of precision*, Physica A **504**, 176 (2018).

[75] Y. V. Nazarov and Y. M. Blanter, *Quantum Transport: Introduction to Nanoscience* (Cambridge University Press, Cambridge, 2009).

[76] J. P. Pekola, P. Solinas, A. Shnirman, and D. V. Averin, *Calorimetric measurement of work in a quantum system*, New J. Phys. **15**, 115006 (2013).

[77] B. Karimi and J. P. Pekola, *Quantum Trajectory Analysis of Single Microwave Photon Detection by Nanocalorimetry*, Phys. Rev. Lett. **124**, 170601 (2020).

[78] A. Kupiainen, P. Muratore-Ginanneschi, J. P. Pekola, and K. Schwieger, *Fluctuation relation for qubit calorimetry*, Phys. Rev. E **94**, 062127 (2016).

[79] B. Donvil, P. Muratore-Ginanneschi, J. P. Pekola, and K. Schwieger, *Model for calorimetric measurements in an open quantum system*, Phys. Rev. A **97**, 052107 (2018).

[80] C. Guarcello, A. Braggio, P. Solinas, G. P. Pepe, and F. Giazotto, *Josephson-Threshold Calorimeter*, Phys. Rev. Applied **11**, 054074 (2019).

[81] S. Gasparinetti, K. L. Viisanen, O.-P. Saira, T. Faivre, M. Arzeo, M. Meschke, and J. P. Pekola, *Fast Electron Thermometry for Ultrasensitive Calorimetric Detection*, Phys. Rev. Appl. **3**, 014007 (2015).

[82] F. Brange, P. Samuelsson, B. Karimi, and J. P. Pekola, *Nanoscale quantum calorimetry with electronic temperature fluctuations*, Phys. Rev. B **98**, 205414 (2018).

[83] B. Karimi, F. Brange, P. Samuelsson, and J. P. Pekola, *Reaching the ultimate energy resolution of a quantum detector*, Nat Commun **11**, 367 (2020).

[84] H.-P. Breuer, *Quantum jumps and entropy production*, Phys. Rev. A **68**, 032105 (2003).

[85] F. W. J. Hekking and J. P. Pekola, *Quantum Jump Approach for Work and Dissipation in a Two-Level System*, Phys. Rev. Lett. **111**, 093602 (2013).

[86] M. Campisi, J. Pekola, and R. Fazio, *Nonequilibrium fluctuations in quantum heat engines: theory, example, and possible solid state experiments*, New J. Phys. **17**, 035012 (2015).

[87] H. Risken and T. Frank, *The Fokker-Planck Equation: Methods of Solution and Applications*, Springer Series in Synergetics (Springer, Berlin, Heidelberg, 1996).

[88] M. B. Plenio and P. L. Knight, *The quantum-jump approach to dissipative dynamics in quantum optics*, Rev. Mod. Phys. **70**, 101 (1998).

[89] L. S. Levitov, H. Lee, and G. B. Lesovik, *Electron counting statistics and coherent states of electric current*, J. Math. Phys. **37**, 4845 (1996).

[90] D. A. Bagrets and Y. V. Nazarov, *Full counting statistics of charge transfer in Coulomb blockade systems*, Phys. Rev. B **67**, 085316 (2003).

[91] C. Flindt, T. Novotný, and A.-P. Jauho, *Full counting statistics of nanoelectromechanical systems*, EPL **69**, 475 (2004).

[92] H. Touchette, *The large deviation approach to statistical mechanics*, Phys. Rep. **478**, 1 (2009).

[93] T. Karzig and F. von Oppen, *Signatures of critical full counting statistics in a quantum-dot chain*, Phys. Rev. B **81**, 045317 (2010).

[94] Y.-F. Chen, D. Hover, S. Sendelbach, L. Maurer, S. T. Merkel, E. J. Pritchett, F. K. Wilhelm, and R. McDermott, *Microwave Photon Counter Based on Josephson Junctions*, Phys. Rev. Lett. **107**, 217401 (2011).

[95] H. J. Carmichael, S. Singh, R. Vyas, and P. R. Rice, *Photoelectron waiting times and atomic state reduction in resonance fluorescence*, Phys. Rev. A **39**, 1200 (1989).

[96] M. Albert, C. Flindt, and M. Büttiker, *Distributions of Waiting Times of Dynamic Single-Electron Emitters*, Phys. Rev. Lett. **107**, 086805 (2011).

[97] D. Dasenbrook, C. Flindt, and M. Büttiker, *Floquet Theory of Electron Waiting Times in Quantum-Coherent Conductors*, Phys. Rev. Lett. **112**, 146801 (2014).

[98] F. Brange, A. Schmidt, J. C. Bayer, T. Wagner, C. Flindt, and R. J. Haug, *Adiabatic-to-nonadiabatic crossover observed in the electron waiting times of a dynamically driven single-electron transistor*, arXiv:2005.06176 [cond-mat.mes-hall] (2020).

[99] N. G. Van Kampen, *Stochastic Processes in Physics and Chemistry*. (Elsevier Science, Burlington, 2011).

[100] G. Haack, M. Albert, and C. Flindt, *Distributions of electron waiting times in quantum-coherent conductors*, Phys. Rev. B **90**, 205429 (2014).

[101] F. Brange, *Quantum Correlations and Temperature Fluctuations in Nanoscale Systems*, Ph.D. thesis, Lund University, Faculty of Science (2019).

[102] I. Klich, *An Elementary Derivation of Levitov's Formula*, in *Quantum Noise in Mesoscopic Physics*, Nato Science Series II, Vol. 97, edited by Y. V. Nazarov (Springer, Netherlands, 2003) pp. 397–402.

[103] S. Redner, R. Metzler, and G. Oshanin, eds., *First-Passage Phenomena And Their Applications* (World Scientific, Singapore, 2014).

[104] S. Singh, É. Roldán, I. Neri, I. M. Khaymovich, D. S. Golubev, V. F. Maisi, J. T. Peltonen, F. Jülicher, and J. P. Pekola, *Extreme reductions of entropy in an electronic double dot*, Phys. Rev. B **99**, 115422 (2019).

[105] T. Fujisawa, T. Hayashi, R. Tomita, and Y. Hirayama, *Bidirectional Counting of Single Electrons*, Science **312**, 1634 (2006).

[106] K. Saito and A. Dhar, *Waiting for rare entropic fluctuations*, EPL **114**, 50004 (2016).

[107] K. Ptaszyński, *First-passage times in renewal and nonrenewal systems*, Phys. Rev. E **97**, 012127 (2018).

[108] M. Khantha and V. Balakrishnan, *First passage time distributions for finite one-dimensional random walks*, Pramana **21**, 111 (1983).

[109] H. Spohn, *Entropy production for quantum dynamical semigroups*, J. Math. Phys. **19**, 1227 (1978).

[110] M. Brunelli, L. Fusco, R. Landig, W. Wieczorek, J. Hoelscher-Obermaier, G. Landi, F. L. Semião, A. Ferraro, N. Kiesel, T. Donner, G. De Chiara, and M. Paternostro, *Experimental Determination of Irreversible Entropy Production in out-of-Equilibrium Mesoscopic Quantum Systems*, Phys. Rev. Lett. **121**, 160604 (2018).

[111] A. Polkovnikov, *Microscopic diagonal entropy and its connection to basic thermodynamic relations*, Ann. Phys. **326**, 486 (2011).

[112] G. Francica, J. Goold, and F. Plastina, *Role of coherence in the nonequilibrium thermodynamics of quantum systems*, Phys. Rev. E **99**, 042105 (2019).

[113] T. E. Humphrey and H. Linke, *Quantum, cyclic, and particle-exchange heat engines*, Physica E Frontiers of Quantum, **29**, 390 (2005).

[114] B. Sothmann, R. Sánchez, and A. N. Jordan, *Thermoelectric energy harvesting with quantum dots*, Nanotechnology **26**, 032001 (2014).

[115] G. Benenti, G. Casati, K. Saito, and R. S. Whitney, *Fundamental aspects of steady-state conversion of heat to work at the nanoscale*, Phys. Rep. **694**, 1 (2017).

[116] H. T. Quan, Y. X. Liu, C. P. Sun, and F. Nori, *Quantum thermodynamic cycles and quantum heat engines*, Phys. Rev. E **76**, 031105 (2007).

[117] K. Brandner, K. Saito, and U. Seifert, *Thermodynamics of Micro- and Nano-Systems Driven by Periodic Temperature Variations*, Phys. Rev. X **5**, 031019 (2015).

[118] K. Zhang, F. Bariani, and P. Meystre, *Quantum Optomechanical Heat Engine*, Phys. Rev. Lett. **112**, 150602 (2014).

[119] P. A. Camati, J. F. G. Santos, and R. M. Serra, *Coherence effects in the performance of the quantum Otto heat engine*, Phys. Rev. A **99**, 062103 (2019).

[120] F. J. Peña, D. Zambrano, O. Negrete, G. De Chiara, P. A. Orellana, and P. Vargas, *Quasistatic and quantum-adiabatic Otto engine for a two-dimensional material: The case of a graphene quantum dot*, Phys. Rev. E **101**, 012116 (2020).

[121] A. Solfanelli, M. Falsetti, and M. Campisi, *Nonadiabatic single-qubit quantum Otto engine*, Phys. Rev. B **101**, 054513 (2020).

[122] B. Karimi and J. P. Pekola, *Otto refrigerator based on a superconducting qubit: Classical and quantum performance*, Phys. Rev. B **94**, 184503 (2016).

[123] A. O. Niskanen, Y. Nakamura, and J. P. Pekola, *Information entropic superconducting microcooler*, Phys. Rev. B **76**, 174523 (2007).

[124] P. A. Erdman, V. Cavina, R. Fazio, F. Taddei, and V. Giovannetti, *Maximum power and corresponding efficiency for two-level heat engines and refrigerators: Optimality of fast cycles*, New J. Phys. **21**, 103049 (2019).

[125] N. Shiraishi, K. Saito, and H. Tasaki, *Universal Trade-Off Relation between Power and Efficiency for Heat Engines*, Phys. Rev. Lett. **117**, 190601 (2016).

[126] N. Shiraishi and K. Saito, *Fundamental Relation Between Entropy Production and Heat Current*, J Stat Phys **174**, 433 (2019).

[127] P. Pietzonka and U. Seifert, *Universal Trade-Off between Power, Efficiency, and Constancy in Steady-State Heat Engines*, Phys. Rev. Lett. **120**, 190602 (2018).

[128] A. C. Barato and U. Seifert, *Thermodynamic Uncertainty Relation for Biomolecular Processes*, Phys. Rev. Lett. **114**, 158101 (2015).

[129] J. M. Horowitz and T. R. Gingrich, *Thermodynamic uncertainty relations constrain non-equilibrium fluctuations*, Nature Phys **16**, 15 (2020).

[130] T. R. Gingrich, J. M. Horowitz, N. Perunov, and J. L. England, *Dissipation Bounds All Steady-State Current Fluctuations*, Phys. Rev. Lett. **116**, 120601 (2016).

[131] T. R. Gingrich, G. M. Rotskoff, and J. M. Horowitz, *Inferring dissipation from current fluctuations*, J. Phys. A **50**, 184004 (2017).

[132] A. Dechant and S.-i. Sasa, *Fluctuation-response inequality out of equilibrium*, arXiv:1804.08250 [cond-mat] (2019).

[133] E. Boukobza and D. J. Tannor, *Three-Level Systems as Amplifiers and Attenuators: A Thermodynamic Analysis*, Phys. Rev. Lett. **98**, 240601 (2007).

[134] V. A. Gerasimov, V. V. Gerasimov, and A. V. Pavlinskiy, *Two Level Metal Vapor Lasers with Thermal Creation of Population Inversion*, Phys. Rev. Lett. **96**, 123902 (2006).

[135] A. A. Clerk, M. H. Devoret, S. M. Girvin, F. Marquardt, and R. J. Schoelkopf, *Introduction to quantum noise, measurement, and amplification*, Rev. Mod. Phys. **82**, 1155 (2010).

[136] N. Linden, S. Popescu, and P. Skrzypczyk, *How Small Can Thermal Machines Be? The Smallest Possible Refrigerator*, Phys. Rev. Lett. **105**, 130401 (2010).

[137] K. E. Dorfman, D. V. Voronine, S. Mukamel, and M. O. Scully, *Photosynthetic reaction center as a quantum heat engine*, PNAS **110**, 2746 (2013).

[138] S.-W. Li, M. B. Kim, G. S. Agarwal, and M. O. Scully, *Quantum statistics of a single-atom Scovil–Schulz-DuBois heat engine*, Phys. Rev. A **96**, 063806 (2017).

[139] A. Ghosh, D. Gelbwaser-Klimovsky, W. Niedenzu, A. I. Lvovsky, I. Mazets, M. O. Scully, and G. Kurizki, *Two-level masers as heat-to-work converters*, PNAS **115**, 9941 (2018).

[140] Y. Zou, Y. Jiang, Y. Mei, X. Guo, and S. Du, *Quantum Heat Engine Using Electromagnetically Induced Transparency*, Phys. Rev. Lett. **119**, 050602 (2017).

[141] A. E. Allahverdyan, R. Balian, and T. M. Nieuwenhuizen, *Maximal work extraction from finite quantum systems*, EPL **67**, 565 (2004).

[142] M. Perarnau-Llobet, K. V. Hovhannisyan, M. Huber, P. Skrzypczyk, N. Brunner, and A. Acín, *Extractable Work from Correlations*, Phys. Rev. X **5**, 041011 (2015).

[143] R. Uzdin and S. Rahav, *Global Passivity in Microscopic Thermodynamics*, Phys. Rev. X **8**, 021064 (2018).

[144] A. Ronzani, B. Karimi, J. Senior, Y.-C. Chang, J. T. Peltonen, C. Chen, and J. P. Pekola, *Tunable photonic heat transport in a quantum heat valve*, Nature Phys **14**, 991 (2018).

[145] D. E. Kirk, *Optimal Control Theory: An Introduction* (Courier Corporation, 2004).

[146] T. Schmiedl and U. Seifert, *Efficiency at maximum power: An analytically solvable model for stochastic heat engines*, EPL **81**, 20003 (2007).

[147] G. De Chiara, T. Calarco, M. Anderlini, S. Montangero, P. J. Lee, B. L. Brown, W. D. Phillips, and J. V. Porto, *Optimal control of atom transport for quantum gates in optical lattices*, Phys. Rev. A **77**, 052333 (2008).

[148] M. Esposito, R. Kawai, K. Lindenberg, and C. Van den Broeck, *Quantum-dot Carnot engine at maximum power*, Phys. Rev. E **81**, 041106 (2010).

[149] B. Andresen, *Current Trends in Finite-Time Thermodynamics*, Angew. Chem. Int. Ed. **50**, 2690 (2011).

[150] E. Aurell, C. Mejía-Monasterio, and P. Muratore-Ginanneschi, *Optimal Protocols and Optimal Transport in Stochastic Thermodynamics*, Phys. Rev. Lett. **106**, 250601 (2011).

[151] A. Dechant, N. Kiesel, and E. Lutz, *Underdamped stochastic heat engine at maximum efficiency*, EPL **119**, 50003 (2017).

[152] V. Cavina, A. Mari, A. Carlini, and V. Giovannetti, *Variational approach to the optimal control of coherently driven, open quantum system dynamics*, Phys. Rev. A **98**, 052125 (2018).

[153] V. Cavina, A. Mari, A. Carlini, and V. Giovannetti, *Optimal thermodynamic control in open quantum systems*, Phys. Rev. A **98**, 012139 (2018).

[154] L. S. Pontryagin, V. G. Boltyanskii, R. V. Gamkrelidze, and E. F. Mishchenko, *The Mathematical Theory of Optimal Processes* (J. Wiley and Sons, New York, 1962).

[155] S. Deffner, *Optimal control of a qubit in an optical cavity*, J. Phys. B **47**, 145502 (2014).

[156] R. Kosloff and T. Feldmann, *Discrete four-stroke quantum heat engine exploring the origin of friction*, Phys. Rev. E **65**, 055102 (2002).

[157] T. Feldmann and R. Kosloff, *Quantum four-stroke heat engine: Thermodynamic observables in a model with intrinsic friction*, Phys. Rev. E **68**, 016101 (2003).

[158] G. Thomas, N. Siddharth, S. Banerjee, and S. Ghosh, *Thermodynamics of non-Markovian reservoirs and heat engines*, Phys. Rev. E **97**, 062108 (2018).

[159] P. Abiuso and V. Giovannetti, *Non-Markov enhancement of maximum power for quantum thermal machines*, Phys. Rev. A **99**, 052106 (2019).

[160] V. Mukherjee, A. G. Kofman, and G. Kurizki, *Anti-Zeno quantum advantage in fast-driven heat machines*, Commun Phys **3**, 1 (2020).

[161] D. Newman, F. Mintert, and A. Nazir, *Quantum limit to nonequilibrium heat-engine performance imposed by strong system-reservoir coupling*, Phys. Rev. E **101**, 052129 (2020).

[162] A. Kato and Y. Tanimura, *Quantum heat current under non-perturbative and non-Markovian conditions: Applications to heat machines*, J. Chem. Phys. **145**, 224105 (2016).

Publication I

P. Menczel and K. Brandner. Limit cycles in periodically driven open quantum systems. *J. Phys. A: Math. Theor.* **52** 43LT01, September 2019.

Publication II

F. Brange, P. Menczel, and C. Flindt. Photon counting statistics of a microwave cavity. *Phys. Rev. B* **99**, 085418, February 2019.

Publication III

S. Singh, P. Menczel, D. S. Golubev, I. M. Khaymovich, J. T. Peltonen, C. Flindt, K. Saito, É. Roldán, and J. P. Pekola. Universal First-Passage-Time Distribution of Non-Gaussian Currents. *Phys. Rev. Lett.* **122**, 230602, June 2019.

Publication IV

P. Menczel, C. Flindt, and K. Brandner. Quantum jump approach to microscopic heat engines. *Phys. Rev. Research* **2**, 033449, September 2020.

Publication V

P. Menczel, C. Flindt, and K. Brandner. Thermodynamics of cyclic quantum amplifiers. *Phys. Rev. A* **101**, 052106, May 2020.

Publication VI

P. Menczel, T. Pyhäranta, C. Flindt, and K. Brandner. Two-stroke optimization scheme for mesoscopic refrigerators. *Phys. Rev. B* **99**, 224306, June 2019.